MASSACHUSETTS INSTITUTE OF TECHNOLOGY

ARTIFICIAL INTELLIGENCE LABORATORY

A.I. Memo No. 440 September 1977

DENSITY RECONSTRUCTION USING ARBITRARY RAY SAMPLING SCHEMES

Berthold K. P. Horn

ABSTRACT.

Methods for calculating the distribution of absorption densities in a cross section through an object from density integrals along rays in the plane of the cross section are well-known, but are restricted to particular geometries of data collection. So-called convolutional-backprojection-summation methods, used now for parallel ray data, have recently been extended to special cases of the fan-beam reconstruction problem by the addition of pre- and post-multiplication steps. In this paper, I present a technique for deriving reconstruction algorithms for arbitrary ray-sampling schemes: the resulting algorithms entail the use of a general linear operator, but require little more computation than the convolutional methods, which represent special cases.

The key to the derivation is the observation that the contribution of a particular ray sum to a particular point in the reconstruction essentially depends on the negative inverse square of the perpendicular distance from the point to the ray and that this contribution has to be weighted by the ray-sampling density. The remaining task is the efficient arrangement of this computation, so that the contribution of each ray sum to each point in the reconstruction does not have to be calculated explicitly.

The exposition of the new method is informal in order to facilitate the application of this technique to various scanning geometries. The frequency domain is not used, since it is inappropriate for the space-variant operators encountered in the general case. The technique is illustrated by the derivation of an algorithm for parallel-ray sampling with uneven spacing between rays and uneven spacing between projection angles.

BACKGROUND AND MOTIVATION.

Recent interest in computerized axial tomography as a means of determining absorption densities in a cross section through an object has led to a variety of basic algorithms [1, 2, 3, 4, 5, 6, 7, 8, 9, 10, 11]. Part of this interest stems from the diagnostic benefits derived by the medical community from scanners utilizing X-ray sources which provide cross sections of the head, body and, soon, the heart. Reconstruction from the mass of data generated by many ray samplings was not feasible before the advent of small, fast computers, and the choice of reconstruction method depends to a large degree on the speed with which such a computer can perform the calculations. As a result the so-called convolutional-backprojection-summation algorithm has emerged as the method of choice and is largely displacing competing methods using two-dimensional Fourier transforms or iterative solution techniques used to solve large sets of sparse equations. These other methods do still find application in specialized areas where speed is not the main criterion of success. A further advantage of the methods based on convolution is that each collection of density integrals, also called a projection, can be treated in a separate computation [6, 11].

Reconstruction methods developed so far, however, have mostly been suited to the parallel-ray projection method of data collection, commonly employed in early, slow computerized axial tomographic scanners [9]. Here density integrals or ray sums are sampled evenly along a line perpendicular to the rays (see figure 1); such a collection of data is called a projection, and projections are formed for a set of projection angles evenly spaced over either 180° or 360°. Reviews of a variety of reconstruction algorithms for this ray-sampling scheme may be found in several references [12, 13, 14].

Since X-rays cannot be focused or deflected as visible light rays can, the pencil beams used for parallel-ray sampling are obtained by tight collimation of radiation emitted from an X-ray source radiating into a large solid angle. Most of the output of the source is therefore wasted. Since a certain number of X-ray photons must be absorbed in order to get a sufficiently accurate estimate of the density integral along the ray, a great deal of time elapses before all ray sums have been observed. In the meantime, the object may have moved. For these and other reasons, modern scanners use fans of rays striking a multiplicity of detectors (see figure 2). A whole projection may now be measured in the time it would have taken to measure a single ray sum with the older system [15, 16].

One difficulty with the so-called fan beam approach is that ray sums are no longer evenly spaced in terms of ray direction and distance of rays from the center of the region being scanned. As a result, conventional reconstruction techniques do not apply without modification. Resorting the ray sums and interpolating to approximate parallel-ray data has not proved very effective, because accuracy is compromised by the interpolation step [15, 16, 17, 18].

Convolutional reconstruction methods have been modified, however, to deal with two very special cases of this ray-sum collection scheme [19, 20, 21]. The first method applies to the situation where the fan is sampled evenly along a line at right angles to the line connecting the source to the center of the region being scanned. Such data collection can be achieved only with a detector array that co-rotates with the source of radiation. This puts a demand for exceptional stability on the central detectors in the array, since points near the center of the region being scanned are

"seen" only by a few detectors during the complete scan [22].

The second method applies to the situation where the detector array lies on a circle about the center of the region being scanned with radius equal to the radius of the circle on which the source moves. This geometry lends itself to the use of a fixed detector array with consequent simplification of the scanner mechanics. Since they lie on the same circle, there is a spatial conflict between the source and the detectors. If they are placed on circles with differing radii, the special case solution no longer applies. The latter geometry is in fact common amongst proposed fast scanners.

Clearly a method is needed for deriving algorithms similar to these modified convolutional methods for data collected by arbitrary sampling of the ray-sum space. Unfortunately, as it turns out, convolutional-backprojection-summation techniques apply only to a few special geometries. Even the two fan-beam reconstruction methods mentioned above augment the convolutional step of the algorithm with a premultiplication of each ray sum by a factor depending on the position of the corresponding ray in the fan. Furthermore, both involve the use of a postmultiplication during the summation step with a factor which depends on the position of the point being reconstructed relative to the fan currently being treated.

While the main impetus for this work comes from the computerized X-ray transverse axial tomography application, similar methods are of importance in such other fields as radio astronomy [2, 3] and electron microscopy [4, 5].

PREVIEW.

The algorithms developed here use general linear operators. Operations using general linear operations can be thought of as spatially varying convolutions, where the "kernel" or "point-spread-function" is allowed to depend on the position at which the operator is applied. The derivation depends on the following observations, which will be elucidated in the next few sections:

* The contribution made by a particular density integral or ray sum to a particular point in the reconstruction is a function of the perpendicular distance from the point to the ray.

* This contribution is essentially proportional to the negative inverse of the square of the distance, except for rays passing very near to the point in question.

* The contribution of a particular ray sum has to be divided by the local ray-sampling density, to account for uneven sampling of the ray-sum space.

* The ray-sampling density is simply the inverse of the Jacobian of the transformation from a convenient uniform scanning coordinated system to the coordinates used in parallel ray reconstruction.

* Using a general linear operator, it is possible to arrange the computation efficiently for most scanning geometries of interest. That is, each generalized projection gives rise to a separate computation and it is not necessary to determine the contribution of each ray sum to each picture cell explicitly.

* For a few special cases, the general linear operator is spatially invariant and thus is simply a convolution. Parallel-ray sampling is the best known example of this.

SOME PRELIMINARY DEFINITIONS.

The notation used here is similar to that used by Lakshminarayanan [19, 6]. The set of rays sampled is a finite subset of the two-parameter family of straight lines in the plane. Various ways can be envisioned for designating particular rays. We may, for example, specify the inclination θ of a ray (relative to the upright axis in figure 3), as well as the perpendicular distance ℓ from the center of the region being scanned. For some scanning geometries, other parameters will be more suitable, but for parallel-ray systems this method is convenient, because, for this case, the projections correspond to evenly spaced values of θ, while rays within a projection correspond to evenly spaced values of ℓ.

Let $p(\ell,\theta)$ be the density integral or ray sum along the ray (ℓ,θ). In practice we will be given only a finite set of these density integrals, corresponding to discrete values of ℓ and θ which depend on the scanning geometry. If we choose to use polar coordinates (r,ϕ) to designate points in the region scanned, and let $f(r,\phi)$ be the absorbing density at the point (r,ϕ), then our task will be to reconstruct values of $f(r,\phi)$, given a set of values of $p(\ell,\theta)$.

One important quantity we will need is the perpendicular distance, t, from a given point to a ray. Using figure 3 again, we get,

$$t = \ell - r\cos(\theta - \phi) \tag{1}$$

If we let ℓ' be the value of ℓ corresponding to $t = 0$, the case of a ray passing directly through the point, then $\ell' = r\cos(\theta - \phi)$, and so

$$t = \ell - \ell' \tag{2}$$

RADON'S FORMULA REVISITED.

The earliest known solution to the reconstruction problem is given by Radon in his paper of 1917 [1]. His result will not be rederived here, since advanced mathematical concepts are needed and because he has given such a clear account of the proof. To apply his formula, we have to assume that $f(r,\phi)$ is bounded, continuous and zero outside the region scanned. Then $p(\ell,\theta)$ will also be zero outside a certain range for ℓ. Further, $p(\ell,\theta)$ will be continuous. Now assume that the partial derivative of $p(\ell,\theta)$ with respect to ℓ is continuous, too. Radon's inversion formula then is [21, 15, 1],

$$f(r,\phi) = \frac{1}{4\pi^2} \int_0^{2\pi} \int_{-\infty}^{+\infty} (-\frac{1}{t}) \frac{\partial}{\partial \ell} p(\ell,\theta)\, d\ell\, d\theta \qquad (3)$$

The above result does not strictly apply if some of the conditions -- particularly the one regarding the continuity of the partial derivative of $p(\ell,\theta)$ -- are violated. We may expect certain artifacts or reconstruction errors in and near regions where the assumptions fail to apply. The magnitude of the resulting errors depends on the details of the numerical approximations made to the above equations.

The inner integral is singular, since $t = 0$, when $\ell = \ell'$ (equation 2). This singular integral may be interpreted as

$$\lim_{\varepsilon \to 0} \int_{-\infty}^{\ell'-\varepsilon} (-\frac{1}{t}) \frac{\partial}{\partial \ell} p(\ell,\theta)\, d\ell + \lim_{\varepsilon \to 0} \int_{\ell'+\varepsilon}^{+\infty} (-\frac{1}{t}) \frac{\partial}{\partial \ell} p(\ell,\theta)\, d\ell \qquad (4)$$

Integrating both terms by parts, we get

$$\lim_{\varepsilon \to 0} \left[\frac{1}{\varepsilon} p(\ell'-\varepsilon,\theta) + \frac{1}{\varepsilon} p(\ell'+\varepsilon,\theta) + \int_{|t| \geq \varepsilon} (-\frac{1}{t^2}) p(\ell,\theta)\, d\ell \right] \tag{5}$$

Since $p(\ell,\theta)$ is assumed to be continuous with respect to ℓ, we can rewrite this

$$\lim_{\varepsilon \to 0} \int_{-\infty}^{+\infty} F_\varepsilon(t)\, p(\ell,\theta)\, d\ell \tag{6}$$

where

$$F(t) = \frac{1}{\varepsilon^2} \qquad \text{for } |t| < \varepsilon \tag{7a}$$

$$= -\frac{1}{t^2} \qquad \text{for } |t| \geq \varepsilon \tag{7b}$$

Combining the above results,

$$f(r,\theta) = \frac{1}{4\pi^2} \int_0^2 \lim_{\varepsilon \to 0} \int_{-\infty}^{+\infty} F_\varepsilon(t)\, p(\ell,\theta)\, d\ell\, d\theta \tag{8}$$

* Clearly each density integral or ray sum $p(\ell,\theta)$ contributes to each point in the reconstruction according to its distance from that point.

* In fact, all but those rays passing very close to the point, contribute with weight proportional to the negative inverse of the square of the distance from the point.

* The weight of the contributions of rays passing near the point is such that the sum of all weights

is zero. That is,

$$\int_{-\infty}^{+\infty} F_{\varepsilon}(t)\, dt = 0 \tag{9}$$

The above three observations are important in the derivation of the new algorithms. The only other problem that will have to be tackled concerns the calculation of ray-sampling density. Then the techniques developed here can be applied to particular scanning geometries.

REVIEW OF THE CONVOLUTIONAL-BACKPROJECTION-SUMMATION METHOD.

Let the inner integral (equation 6) discussed in the previous section be called $g(\ell',\theta)$. Clearly it can be thought of as a convolution of the original projection data $p(\ell,\theta)$ with the filter function $F_\varepsilon(t)$, since $t = \ell' - \ell$ and $F_\varepsilon(t)$ are symmetric:

$$g(\ell',\theta) = \lim_{\varepsilon\to 0} \int_{-\infty}^{+\infty} F_\varepsilon(\ell' - \ell)\, p(\ell,\theta)\, d\ell \tag{10}$$

We can then use the outer integral (equation 8) to calculate the densities from this convolved or filtered data:

$$f(r,\phi) = \frac{1}{4\pi^2} \int_0^{2\pi} g(\ell',\theta)\, d\theta \tag{11}$$

In practice we know only a finite number of ray sums and consequently have to approximate both of the above integrals by finite sums. If we choose to observe M projections evenly spaced in angle from $\theta = 0$ to $\theta = 2\pi$, we may approximate the outer integral (equation 11) by

$$f(r,\theta) \simeq \frac{1}{4\pi^2} \sum_{j=0}^{M-1} g_j(\ell')\, \delta\theta \tag{12}$$

where $\delta\theta = (2\pi)/M$ is the angular increment between successive projections. Note that $g_j(\ell')$ is the convolved projection data of the j^{th} projection evaluated at $\ell' = r\cos(\theta - \phi)$. For reasons of computational efficiency, we calculate the convolved data at only a small number of places -- typically the same ones for which projection data is available. This allows the use of a single convolution per projection, independent of the location of the points

in the reconstruction. The value of $g_j(\ell')$, needed in the above summation, must however then be estimated by interpolation from the values at those places where the convolution was actually computed.

This convolution will be discussed next. If we let W be the width or diameter of the region being scanned, and N the number of evenly spaced rays across this width (sampled by the detectors) we can approximate the inner integral (equation 10) by

$$g_{i'j} = \sum_{i=0}^{N-1} F_{i'-i}\, p_{ij}\, \delta\ell \tag{13}$$

where $\delta\ell = W/(N-1)$ is the uniform interval between successive rays in a projection and p_{ij} is the ray sum for the i^{th} ray in the j^{th} projection (see figure 4). Now the i'^{th} ray passes at a distance $\ell' = i'\,\delta\ell - W/2$ from the origin, so this is the value of ℓ' associated with $g_{i'j}$. From this relationship one can determine which values of $g_{i'j}$ should be used in the interpolation for estimating $g_j(\ell')$. One uses $g_{i'j}$ and $g_{(i'+1)j}$ where

$$i' = \left\lfloor (\ell' + W/2)/\delta\ell \right\rfloor \tag{14}$$

We next turn our attention to the discrete approximation to $F_\varepsilon(t)$ (equation 7),

$$F_k = -\frac{w_k}{(k\,\delta\ell)^2} \qquad \text{for } k \neq 0 \tag{15a}$$

$$F_0 = -2\sum_{k=1}^{\infty} F_k \tag{15b}$$

The value of F_0 is chosen simply so that the sum of all filter coefficients is zero, in view of a similar condition on $F_\varepsilon(t)$ (equation 9).

The weights, w_k, give some flexibility in the numerical approximation to the singular integral (equation 10). Some common choices are:

1. Ramachandran & Lakshminarayanan (1971)

$$w_k = 2 \text{ for } k \text{ odd, and } w_k = 0 \text{ for } k \text{ even} \tag{16}$$

2. Shepp & Logan (1974)

$$w_k = 4k^2/(4k^2 - 1) \tag{17}$$

3. Horn (1976)

$$w_k = 1 \tag{18}$$

The third set of weights corresponds to the trapezoidal rule for numerical integration or quadrature. Linear combinations of the above weights may also be used. For example, a combination of (1/3) of the first set and (2/3) of the third set produces weights which are alternately (2/3) and (4/3). This corresponds to Simpson's well-known rule for numerical quadrature. The second set of weights on the other hand corresponds to a numerical integration formula which takes into account the singular nature of the integral being approximated, as will be shown later.

By summing the series indicated (equation 15b), one finds that $(\delta\ell)^2 F_0 = \pi^2/2$, 4 and $\pi^2/3$ for the three sets of weights suggested.

CHOICE OF WEIGHTS.

This analysis differs from the standard derivation of the weights w_k. These coefficients are commonly obtained by inverse Fourier transformation from a filter response designed in the frequency domain. Their differences are usually discussed in a somewhat ad hoc fashion in terms of the need to low-pass filter the projection data in order to avoid aliasing or under-sampling. Clearly, this is wrong, since to avoid the effects of under-sampling, low-pass filtering has to be performed before sampling. After sampling we throw out the good with the bad, since they are no longer distinguishable. (Fortunately, the finite size of the detectors and to some extent the finite size of the source of radiation, account for some low-pass filtering of the projection data before sampling and thus help to limit the magnitude of the resulting artifacts).

The derivation of these weights as coefficients in formulae for numerical quadrature instead seems more insightful. The connection between these two points of view is made by Hamming [23, 24] in his discussion of the frequency response of integration formulae.

Different choices of weights lead to different approximation behavior. As one might expect, there is a trade-off between noise and resolution. Random additive noise in the density integrals leads to noise in the final reconstruction. The amplification factor depends on not only the details of scanning geometry (number of projections and number of rays per projection), but also the weights chosen. The first filter above (equation 16), for example, has fine resolution at the cost of sensitivity to noise and sharp contrasts, makes full use of the sampled projection and does not attenuate higher frequencies. The third filter, on the other hand (equation 18) lies

at the other extreme and tends to blur sharp edges, while suppressing noise; it removes some of the higher frequency components of the sampled projection data. The second filter (equation 17) lies between the two extremes. In practice, one should allow for the possibility of using different weights to suit different applications, in order to be able to exploit fully the trade-off between noise amplification and resolution.

Overshoot in regions where $p(\ell,\theta)$ does not have a continuous derivative with respect to ℓ is a common problem with filters that produce high resolution results. They are most sensitive to violations of the assumptions underlying Radon's inversion formula.

Finally, note that the two summations (equations 12 and 13) allow us to evaluate the estimated density at arbitrary points (r,ϕ). In practice, one uses a fixed grid of picture cells, in the form of some regular tesselation of the plane. This limits the amount of computation and reflects the fact that resolution is limited, in any case, by the sampling width $(\delta\ell)$ along each projection, and that no new information is gained by performing reconstruction on a grid much finer than this.

RAY-SAMPLING DENSITY.

With the parallel-ray scheme described, sampling is uniform in ℓ and θ. That is, successive rays in a particular projection correspond to evenly spaced values of ℓ, while successive projections correspond to evenly spaced values of θ. Thus ℓ and θ are natural coordinates for the rays. Other coordinates are preferred when we are dealing with fan beams or more general scanning schemes. Essentially, whatever the scanning scheme, we must find coordinates ξ and η natural to the particular geometry, such that we have uniform sampling in ξ and η. The collection of ray sums $p(\ell,\theta)$ for a fixed value of η will be referred to as a generalized projection. It is simple now to rewrite the reconstruction formula (equation 8) as follows:

$$f(r,\phi) = \frac{1}{4\pi^2} \lim_{\varepsilon \to 0} \int\int F_\varepsilon(t)\, p(\ell,\theta)\, J\, d\xi\, d\eta \tag{19}$$

where,

$$J = \frac{\partial \ell}{\partial \xi}\frac{\partial \theta}{\partial \eta} - \frac{\partial \theta}{\partial \xi}\frac{\partial \ell}{\partial \eta} \tag{20}$$

is the Jacobian of the transformation from (ξ,η) space to (ℓ,θ) space. It can be conveniently visualized as the factor by which a small area in (ξ,η) space is expanded when mapped into (ℓ,θ) space (see figure 5).

Since we have uniform sampling in (ξ,η) space, the sampling density in (ℓ,θ) space equals the uniform density divided by J. To see this more clearly, let two rays (ℓ,θ) and (ℓ',θ') be considered "near" each other if $|\ell - \ell'| < \delta\ell/2$ and $|\theta - \theta'| < \delta\theta/2$. Clearly then the number of rays "near" a given ray is proportional to $(1/J)\ \delta\ell\ \delta\theta$.

* Consequently, we can state that the ray-sampling density is inversely proportional to J.

* Further, it is clear that the contribution of a particular ray sum to a particular point must be weighted by J, that is, the inverse of the ray-sampling density.

Intuitively, this seems reasonable since we do not want to emphasize contributions from regions of (ℓ,θ) space which happen to be sampled more densely than others. It should be noted that we can no longer expect all regions of the reconstruction to be equally well determined or resolved, since rays important to the reconstruction of one may be sampled more coarsely than the others. Fortunately, for practical fan-beam systems, the equivalent change in point-spread function over the region being reconstructed tends to be fairly small and thus not visually noticeable.

We may write (equation 19):

$$f(r,\phi) = \frac{1}{4\pi^2} \int g(r,\phi,\eta)\, d\eta \tag{21}$$

where

$$g(r,\phi,\eta) = \lim_{\varepsilon \to 0} \int F_\varepsilon(t)\, J(\xi,\eta)\, p(\xi,\eta)\, d\xi \tag{22}$$

In the general case, $t = \ell - \ell'$ will be a function of both (r,ϕ) and (ξ,η). As a result, the inner integral may have to be evaluated separately for every point (r,ϕ) in the reconstruction, for every projection. That is, g is a function of three variables, unless we further restrict the possible scanning

schemes. Fortunately, in most interesting cases a variable $\chi(r,\phi)$ can be introduced which is natural to the scanning scheme such that g becomes a function of χ and η only. (This may require splitting the variable t into a product of a term which depends on ξ and one which does not -- the latter term can be moved out of the inner integral.

If g can be written in terms of χ and η only, a great computational efficiency arises, because the inner integral has to be evaluated only for every $\chi(r,\phi)$ for a given projection, not separately for every picture cell (r,ϕ). An example later on will make this clear. Frequently, a good choice for $\chi(r,\phi)$ is ξ' defined by the equation $\ell(\xi') = \ell'$.

GENERAL LINEAR OPERATORS.

If we can find a new parameter $\chi(r,\phi)$ as described above, then the inner integral (equation 22) becomes

$$g(\chi,\eta) = \int F_{\varepsilon}[t(\chi,\xi,\eta)]\ J(\xi,\eta)\ p(\xi,\eta)\ d\xi \tag{23}$$

If we consider η as a parameter for the moment we can write this in a form that is more easily recognized:

$$g_{\eta}(\chi) = \int K_{\eta}(\chi,\xi)\ p_{\eta}(\xi)\ d\xi \tag{24}$$

This is a general linear operation with kernel $K_{\eta}(\chi,\xi) = F_{\varepsilon}(t)\ J$. This operation is very similar to a convolution aside from the fact that in a convolution the kernel would be invariant. The above integral may also be referred to as a superposition integral and the general linear operator may also be called a linear space-variant operator. Integrals of similar form occur in the solution of partial differential equations, in which case the kernel is called a Green's function. In a number of special cases, such as uniform, parallel-ray scanning, the kernel is space-invariant (that is, is a function of $\chi - \xi$ only) and the operation simply becomes a convolution.

Note, by the way, that the sampling-density factor, J, presents no special problems, representing merely a pre-multiplication of the ray sums. In fact, under fairly general conditions, J is a function of ξ only and so each ray sum is simply multiplied by a factor depending on its position within its generalized projection.

PARALLEL-RAY SCANNING WITH VARIABLE RAY- AND PROJECTION-ANGLE SPACING.

As an illustration of the utility of the new method for finding reconstruction algorithms, we develop an algorithm suited to parallel-ray scanning where both the spacing between successive rays in a projection and the interval between successive projection angles are non-uniform.

Let the rays be evenly spaced in ξ, while projections are evenly spaced in η. Then we write ℓ as a function of ξ, and we write θ as a function of η. Clearly, $\ell(\xi)$ and $\theta(\eta)$ should be monotonically increasing, continuous and differentiable. This also assures us that the inverse functions will exist. That is, given ℓ we can find ξ, and given θ we can find η. The Jacobian (equation 20), here simplifies to:

$$J = \frac{\partial \ell}{\partial \xi} \frac{\partial \theta}{\partial \eta} \tag{25}$$

It is clear given these assumptions that J will be positive and that its two factors may be split between the inner and outer integrals. Now choose ξ', such that $\ell(\xi') = \ell'$, that is (equations 1 and 2),

$$\ell(\xi') = r \cos [\theta(\eta) - \phi] \tag{26}$$

Then, $t = \ell(\xi) - \ell(\xi')$ and consequently we find that the inner integral is a function of ξ' and η only. Finally (from equations 21 and 22),

$$f(r,\phi) = \frac{1}{4\pi^2} \int g(\xi',\eta) \frac{\partial \theta}{\partial \eta} \, d\eta \tag{27}$$

where

$$g(\xi',\eta) = \lim_{\varepsilon \to 0} \int F_\varepsilon(\ell - \ell') \, p(\xi,\eta) \frac{\partial \ell}{\partial \xi} \, d\xi \tag{28}$$

Here then we have an inner integral which corresponds to a general linear operation. It becomes a convolution only if ℓ happens to be a linear function of ξ, that is, when the spacing of the rays in a given projection is uniform.

For discrete sampling of the ray sums we approximate the above integrals by sums:

$$f(r,\phi) \simeq \frac{1}{4\pi^2} \sum_j g_j(\xi') \, \delta\theta_j \tag{29}$$

$$g_{i'j} = \sum_i F_{i'i} p_{ij} \, \delta\ell_i \tag{30}$$

Here again, p_{ij} is the i^{th} ray sum in the j^{th} projection. If θ_j is the j^{th} projection angle and ℓ_i is the distance of the i^{th} ray from the center of the region being scanned, then $\delta\theta_j$ is the angular interval associated with a particular projection, while $\delta\ell_i$ is the projection interval associated with a particular ray, where

$$\delta\theta_j = (\theta_{j+i} - \theta_{j-i})/2 \quad \text{and} \quad \delta\ell_i = (\ell_{i+1} - \ell_{i-1})/2 \tag{31}$$

Also,

$$F_{i'i} = -\frac{w_{i'-i}}{(\ell_i - \ell_{i'})^2} \qquad \text{for } i \neq i' \tag{32a}$$

$$F_{i'i'} \delta\ell_{i'} = \sum_{i \neq i'} F_{i'i} \, \delta\ell_i \tag{32b}$$

That is, F_{ii} is chosen so that

$$\sum_i F_{i'i} \, \delta\ell_i = 0 \tag{33}$$

Here we happen to calculate $g_{i'j}$ for a set of values of ℓ' which corresponds to the set of values of ℓ for rays whose ray sum is known. One could equally well have decided to perform the calculation for a different, perhaps evenly spaced set of values of ℓ'. In either case, the values $g_j(\ell')$ have to be found from the known $g_{i'j}$ by interpolation as indicated before.

Note that the inner sum (equation 30) is not a convolution, but a general linear sum. Fortunately, it requires little more calculation than a simple convolution. It is also clear how the above simplifies if either the ray spacing or the projection-angle spacing becomes uniform.

It should be pointed out that there is a minor practical problem due to the slow convergence of the series (equation 32b) for $F_{i'i'}$. When rays are spaced evenly, this sum can be found analytically (equation 15b), while it is likely that numerical techniques are required here. If ℓ is asymptotically linearly related to ξ, then the error term of the sum evaluated with n terms is proportional to $1/n$. This illustrates the problem as well as suggests a solution. If we let s_n be the sum of $F_{i'i}\delta\ell_i$ from $i = i'-n$ to $i = i'+n$, then a good estimate of the sum from $i = -\infty$ to $i = +\infty$ is given by

$$s_\infty \simeq (n+1)\, s_{n+1} - (n)\, s_n \qquad (34)$$

TAKING INTO ACCOUNT THE SINGULAR NATURE OF THE INNER INTEGRAL.

So far, when we approximate the inner integral (equation 28) by the sum (equation 30), we pay little heed to the singular nature of the kernel $F_\varepsilon(\ell - \ell')$. It is reasonable to suppose that better approximations may be found by considering methods which deal with the singularity. In this regard we note first that the values of the density integral $p(\xi,\eta)$ are known only at discrete points, and that it is reasonable to assume that this component of the integrand varies relatively slowly over small distances along a projection (in fact, the partial derivative of this function was assumed to be continuous). The term $(-1/t^2)$ on the other hand is known everywhere but varies rapidly near the point $t = 0$. We can make use of these observations after splitting the inner integral into many integrals, each over the width of one detector.

Let the i^{th} detector intercept rays lying in the beam between ℓ_i and ℓ_{i+1} (see figure 6). It measures the density integral p_{ij} in the j^{th} projection. Further, let

$$\ell' = (\ell_{i'} + \ell_{i'+1})/2 \tag{35a}$$

and

$$\varepsilon = (\ell_{i'+1} - \ell_{i'})/2 \tag{35b}$$

[Note that here the center of the i^{th} detector lies at $(\ell_i + \ell_{i+1})/2$].
The inner integral (equation 28) can then be written as:

$$\sum_{i=-\infty}^{i'-1} \int_{\ell_i}^{\ell_{i+1}} \left(-\frac{1}{t^2}\right) p(\ell,\theta)\, d\ell + \int_{\ell_{i'}}^{\ell_{i'+1}} \left(\frac{1}{\varepsilon^2}\right) p(\ell,\theta)\, d\ell + \sum_{i=i'+1}^{+\infty} \int_{\ell_i}^{\ell_{i+1}} \left(-\frac{1}{t^2}\right) p(\ell,\theta)\, d\ell \tag{36}$$

Now note that $t = (\ell - \ell')$ and

$$\int_{\ell_i}^{\ell_{i+1}} -\frac{1}{(\ell - \ell')^2}\, d\ell = \frac{1}{(\ell_{i+1} - \ell')} - \frac{1}{(\ell_i - \ell')} = -\frac{(\ell_{i+1} - \ell_i)}{(\ell_{i+1} - \ell')(\ell_i - \ell')} \qquad (37)$$

If we use this result and replace $p(\ell,\theta)$ with p_{ij}, when $\ell_i \leq \ell < \ell_{i+1}$, then the inner integral (equation 36) becomes

$$g_{i'j} = \frac{4}{(\ell_{i'+1} - \ell_{i'})} p_{i'j} - \sum_{i \neq i'} \frac{(\ell_{i+1} - \ell_i)}{(\ell_{i+1} - \ell')(\ell_i - \ell')} p_{ij} \qquad (38)$$

The reader may verify that this in fact reduces to Shepp and Logan's method (equation 17) when rays are evenly spaced [that is, when $\ell_i = (i - 1/2)\delta\ell - W/2$, $\delta\ell = W/(N - 1)$]. More complicated integration formulae may be developed if one fits low-order polynomials to the values of p_{ij} instead of assuming that the density integrals are constant over the width of one detector. Techniques for doing this may be found in standard texts on numerical analysis [23]. Here, however, we will be satisfied with the simple form developed above (equation 38) which is better than the method developed earlier (equation 30) since there is no difficulty in finding the weights by which the ray sums are to be multiplied.

The method can be further simplified by using the other form (equation 37) of the integral of $(-1/t^2)$:

$$\sum_{i=-\infty}^{i'-1} \left[\frac{1}{(\ell_{i+1} - \ell')} - \frac{1}{(\ell_i - \ell')}\right] p_{ij} + \frac{4}{(\ell_{i'+1} - \ell_{i'})} p_{i'j} + \sum_{i=i'+1}^{+\infty} \left[\frac{1}{(\ell_{i+1} - \ell')} - \frac{1}{(\ell_i - \ell')}\right] p_{ij} \qquad (39)$$

Splitting both sums and rearranging terms leads to the surprisingly simple result,

$$g_{i'j} = - \sum_{i} \frac{(p_{ij} - p_{(i-1)j})}{(\ell_i - \ell')} \tag{40}$$

The reader may want to compare this with the original form of the inner integral (equation 4), from which this result can also be obtained directly. This numerical approximation of the inner integral is particularly advantageous from a computational point of view since it is no longer necessary to keep a two-dimensional array of pre-calculated weights. This assumes that one can afford to calculate $(\ell_i - \ell')$, and that the ray sums are replaced by the differences of ray sums as required above (equation 40). This latter calculation is needed only once per projection.

The form of the result also implies that reconstruction may be possible when the ray spacing varies discontinuously, that is, when $\ell(\xi)$ does not have a continuous derivative with respect to ξ. This in turn suggests the possibility of using evenly spaced detectors; combining the measurements of neighboring detectors in portions of the projection where high resolution is not required.

MOTIVATION FOR STUDYING VARIABLE RESOLUTION METHODS.

In a number of situations, one is intested in reconstructing as object buried inside some larger entity of less interest. If one were simply to restrict the scanned region to the object of interest, correct reconstructions would not be obtained, since the absorbing density is then non-zero outside the region being scanned. This violates assumptions underlying Radon's formula. Up to now, the only alternative was to scan the whole region occupied by absorbing material and reconstruct it with uniform resolution. (At best, there is some saving in the backprojection step, since one need not calculate the density of picture cells outside the region of interest).

The new variable resolution method to be illustrated here has the advantage that the computation of the filtered projection is speeded up considerably since fewer ray sums have to be measured. Of equal importance may be the fact that less radiation is needed to obtain this smaller set of measurements.

DEMONSTRATION OF THE VARIABLE RESOLUTION METHOD.

In order to illustrate some of the features of the new method, a computer algorithm based on the results derived here (equations 40 and 29) has been developed. This algorithm has been applied to ray sums calculated from a mathematically defined object or phantom composed of elliptical parts (see figure 7). A comparison will be made of the results obtained in three cases:

(a) .N = 200 evenly spaced rays, 2 mm apart.

(b) N = 100 evenly spaced rays, 2 mm apart at the center, 8 mm at the edge.

(c) N = 100 evenly spaced rays, 4 mm apart.

In order that the comparison be fair, all other parameters were held constant. The region scanned had a diameter W = 400 mm, and M = 150 projection angles were employed in each case. For case B, the following transformation from uniform scanning coordinates to actual scanning coordinates was used:

$$\ell = \frac{W}{2}\left(\frac{\xi}{2}\right)\left(1 + \xi^2\right) \qquad (41)$$

where $-1 \leq \xi \leq +1$. In all cases the ray sums were averages obtained by integrating from the left edge of a beam striking a detector to the right edge of this beam so as to simulate the suppression of high frequency components obtained in practice as a result of the finite width of the detectors.

Each projection is first processed to produce the differences required in the summation (equation 40). The filtered sums are then determined for positions corresponding to the individual detectors. In order to facilitate

back-projection, these values are (linearly) interpolated to a much finer, evenly spaced set of positions. Backprojection proceeds much as it does for convolutional algorithms by processing each picture cell in turn. For every picture cell, the appropriate point in the interpolated filtered data is found by considering the projection angle (as illustrated in figure 4). The value found there is then added into the sum accumulated for this picture cell so far. The whole process is repeated for all projection angles.

The picture cells were spaced 1.5 mm and lay inside a circle of diameter 330 mm for the reconstructions shown in figures 8 and 9. For the reconstructions shown in figures 10 and 11, the spacing was .75 mm inside a circle of 150 mm diameter.

The time required for backprojection was essentially the same for the three cases, while the time for the general linear operation in cases B and C was about one quarter that required for case A, as expected.

ANALYSIS OF RECONSTRUCTION RESULTS.

The low resolution near the edge of the region of reconstruction (where the rays are spaced 8 mm apart) of method B can best be seen in figure 8. Not much is visible in this figure of the central components however. Figure 9 more clearly shows the low overall resolution of method C. (It is important not to be misled by the apparent high resolution of high contrast features due only to the reduced density scale of this mode of presentation). The good resolution of method B in the central regions is illustrated by figure 10, as well as by the density profiles in figure 11. The density profiles are along the lines indicated in figure 12. It appears that while the variable resolution method, B, requires only about as much computation as the low resolution method, C, it has about as much central resolution as the high resolution method, A.

The reader will have noticed the reconstruction artifacts particularly apparent in the high contrast presentations (figures 9 and 10). The phantom was purposefully constructed to include high contrast features outside a central region with a variety of low contrast features, since artifacts radiating outwards from the former often degrade the presentation of the latter.

As indicated earlier, these artifacts are due to the projection data's failure to obey the assumptions underlying Radon's formula. That is, the partial derivative of $p(\ell,\theta)$ with respect to ℓ is not everywhere continuous. It is easy to see that the discontinuities occur at the edges of the elliptical components of the phantom and that line-like artifacts oriented tangentially to the high-contrast components radiate across the reconstructed density distribution. The exact magnitude of these artifacts depends on the particular

alignment of a projected edge relative to the edges of the detectors. It is easy to see, too, that the magnitude of these effects varies inversely with the number of projection angles, since the contribution of each projection varies in this way. Further, it can be shown that the magnitude of this effect also decreases with the number of rays in a projection. The artifacts are visible in the examples presented here because both the number of projection angles (150) and the number of rays per projection (100 or 200) are relatively small and because of the strong contrast between some of the large features in the phantom.

The important point is that these artifacts, while visible, do not mask the low contrast detail in the center, and that the magnitude of the artifacts in the central region are not significantly larger in the reconstruction obtained using method B, than they are in those obtained using method A. The new method would be of less interest if this were not the case.

SUMMARY AND CONCLUSIONS.

A technique has been developed for finding reconstruction methods for arbitrary ray-sampling schemes. The algorithms use a general linear operator, the kernel of which depends on the particular scanning geometry. It is suggested here that the kernel coefficients can be fruitfully considered as weights in a method for numerical quadrature of an integral. In a few special cases, the kernel is a function of the difference of coordinates only, and the general linear operation becomes simply a convolution. In this case, the algorithm essentially reduces to the familiar convolution-backprojection-summation method.

As an illustration of the more general case, an algorithm was derived which applies to parallel-ray data when the spacing of rays in a projection is uneven and the projections are spaced unevenly in angle. The new method requires little more computation than does the convolutional method.

Importantly, the Fourier transform is not used in the derivation. Indeed, it does not apply to the linear space-variant systems that occur in the general case, and also in particular cases of practical importance. A future paper will explore the application of this general method to a variety of fan-beam scanning geometries suitable for modern tomographic machines.

REFERENCES.

1. J. Radon, "Uber die Bestimmung von Funktionen durch ihre Integralwerte langs gewisser Mannigfaltigkeiten," Berichte Saechsische Akademie der Wissenschaften, Vol. 69, pp. 262-279, 1917.

2. R. N. Bracewell, "Strip integration in radio astronomy," Aust. Jour. of Phys., Vol. 9, pp. 198-217, 1960.

3. R. N. Bracewell & A. C. Riddle, "Inversion of fan-beam scans in radio astronomy," The Astrophysical Journal, Vol. 150, pp. 427-434, 1967.

4. D. De Rosier & A. Klug, "Reconstruction of three-dimensional structures from electron micrographs," Nature, Vol. 217, pp. 130-138, 1968.

5. R. A. Crowther, D. J. De Rosier & A. Klug, "The reconstruction of a three-dimensional structure from projections and its application to electron microscopy," Proc. Roy. Soc., London, Ser. A, Vol. 317, pp. 319-340, 1970.

6. G. N. Ramachandran & A. V. Lakshminarayanan, "Three-dimensional reconstruction from radiographs and electron micrographs: Application of convolution instead of Fourier transforms," Proc. Nat. Acad. Sci. U.S., Vol. 68, pp. 2236-2240, 1970.

7. B. K. Vainshtein, "Finding the structure of objects from projections," Sov. Phys.-Crystallogr., Vol. 15, pp. 781-787, 1971.

8. A. M. Cormack, "Reconstruction of densities from their projections with applications to radiological physics," Physics in Medicine and Biology, Vol. 18, pp. 195-207, 1973.

9. G. N. Hounsfield, "Computerized transverse axial scanning (tomography): Part I. Description of system," Brit. Jour. Radiology, Vol. 46, pp. 1016-1022, 1973.

10. Robert B. Marr, "On the reconstruction of a function on a circular domain from sampling of its line integrals," Jour. of Math. Anal. and Appli., Vol. 45, pp. 357-374, 1974.

11. L. A. Shepp & B. F. Logan, "The Fourier reconstruction of a head section," IEEE Trans. Nucl. Sci., Vol. NS-21, pp. 21-43, 1973.

12. R. Gordon & G. T. Herman, "Three-dimensional reconstruction from projections: A review of algorithms," Int. Review of Cytology, Vol. 38, pp. 111-151, 1974.

13. R. M. Mersereau & A. V. Oppenheim, "Digital reconstruction of multi-dimensional signals from their projections," Proc. of the IEEE, Vol. 62, pp. 1319-1338, 1974.

14. R. A. Brook, & G. Di Chiro, "Principles of computer assisted tomography in radiographic and radio-isotopic imaging," Phys. Med. Biol., Vol. 21, pp. 689-732, 1976.

15. J. W. Beattie, "Tomographic reconstruction from fan beam geometry using Radon's integration method," IEEE Trans. on Nucl. Sci., Vol. NS-22, pp. 359-363, 1975.

16. Z. H. Cho & J. K. Chan, "A comparative study of 3-D image reconstruction algorithms with reference to number of projections and noise filtering," IEEE Trans. on Nucl. Sci., Vol. NS-22, pp. 344-358, 1975.

17. L. Wang and Z. H. Cho, "3-D reconstruction algorithms for fan beam scans," Image Processing for 2-D and 3-D Reconstruction from Projections, WB-61-64, Topical Meeting of the Optical Society, August 4-7, 1975, Stanford, 1975.

18. P. Dreike & D. P. Boyd, "Convolution reconstruction of fan beam projections," Computer Graphics and Image Processing, Vol. 5, pp. 459-469, 1976.

19. A. V. Lakshminarayanan, "Reconstruction from divergent ray data," TR-92, Dept. of Computer Science, State University of New York, Buffalo, 1975.

20. Lily Wang, "Three-dimensional reconstruction with a fan beam scanning geometry, ATR-75(8139)-2, The Aerospace Corporation, El Segundo, CA, 1975.

21. G. T. Herman, A. V. Lakshminarayanan, A. Naparstek, E. L. Ritman, R. A. Robb, & E. H. Wood, "Rapid computerized tomography," in Medical Data Processing, London: Taylor & Francis Ltd., 1976, pp.

22. G. Kowalski, "Reconstruction of objects from their projections: the influence of measurement errors on the reconstruction," IEEE Tran. on Nucl. Sci., NS-24, pp. 850-864, 1977.

23. R. W. Hamming, Numerical Methods for Scientists and Engineers, New York: McGraw-Hill, 1972, pp. 323-330.

24. R. W. Hamming, Digital Filters, Englewood Cliffs, N.J.: Prentice-Hall, pp. 37-41, 1977.

FIGURE CAPTIONS.

Figure 1. Parallel-ray scanning geometry. Many projections are measured, each with rays arriving in a particular direction.

Figure 2. Fan-beam scanning geometry. Many projections are measured, each with the source in a particular position.

Figure 3. Designation of particular rays and calculation of distance between a ray and a point in the region being scanned.

Figure 4. Detailed geometry of a parallel ray projection.

Figure 5. Transformation from uniform scanning coordinates to coordinates used in Radon's inversion formula. The Jacobian is the ratio of the area of the quadrilateral A'B'C'D' to that of ABCD.

Figure 6. Positions of detectors along projection as defined in derivation of numerical approximation to singular integral.

Figure 7. Outlines of the elliptical components of the phantom used in the demonstration of the variable resolution method. The numbers indicate the absorbing densities of the components.

Figure 8. Reconstructions obtained in the following three cases:

(A) 200 evenly spaced rays

(B) 100 unevenly spaced rays

(C) 100 evenly spaced rays

In this figure black corresponds to a density of -.06, while white corresponds to a density of 1.22.

Figure 9. The same reconstructions as in previous figure displayed with higher contrast. Here black corresponds to a density of .94, while white corresponds to a density of 1.06.

Figure 10. Higher resolution display of central regions of the reconstructions shown in previous figures.

Figure 11. Horizontal density profiles through the middle of the central circular component of each of the three reconstructions. While method B requires only about as much computation as method C, it gives rise to resolution about as good as method A.

Figure 12. Lines along which density profiles of previous figure were taken.

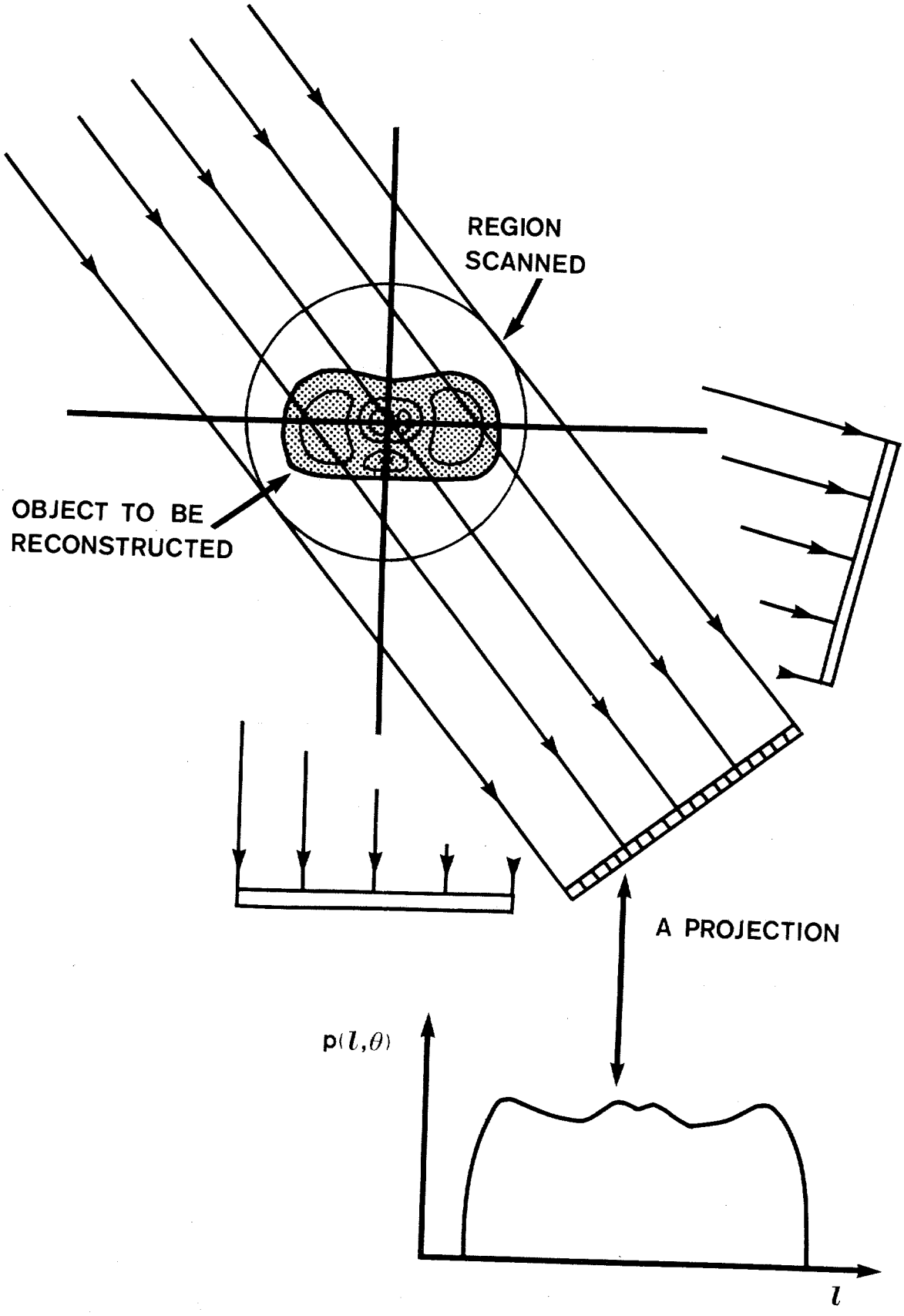
REGION
SCANNED
OBJECT TO BE
RECONSTRUCTED
A PROJECTION
p(l,θ)
l

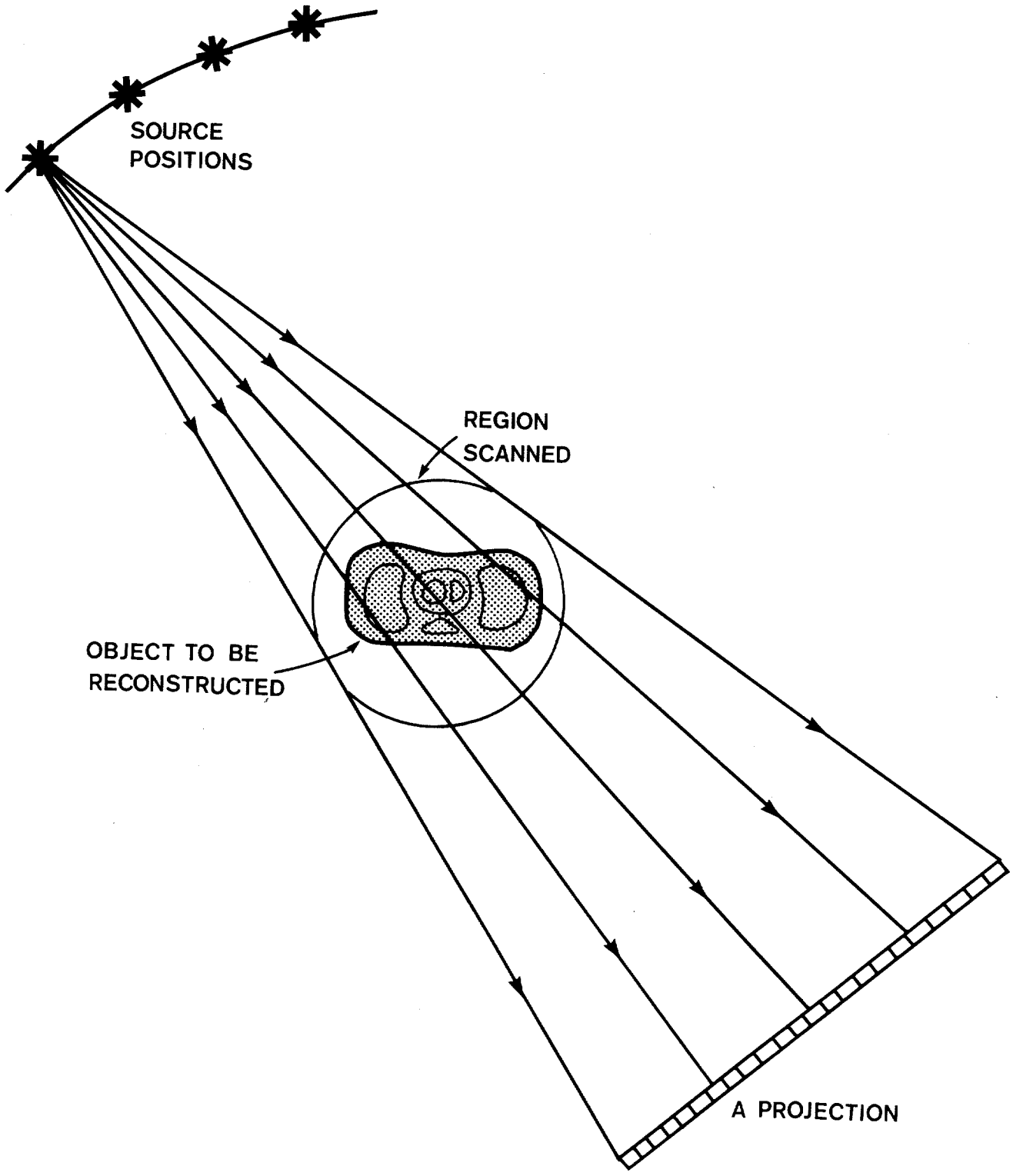
SOURCE
POSITIONS
REGION
SCANNED
OBJECT TO BE
RECONSTRUCTED
A PROJECTION

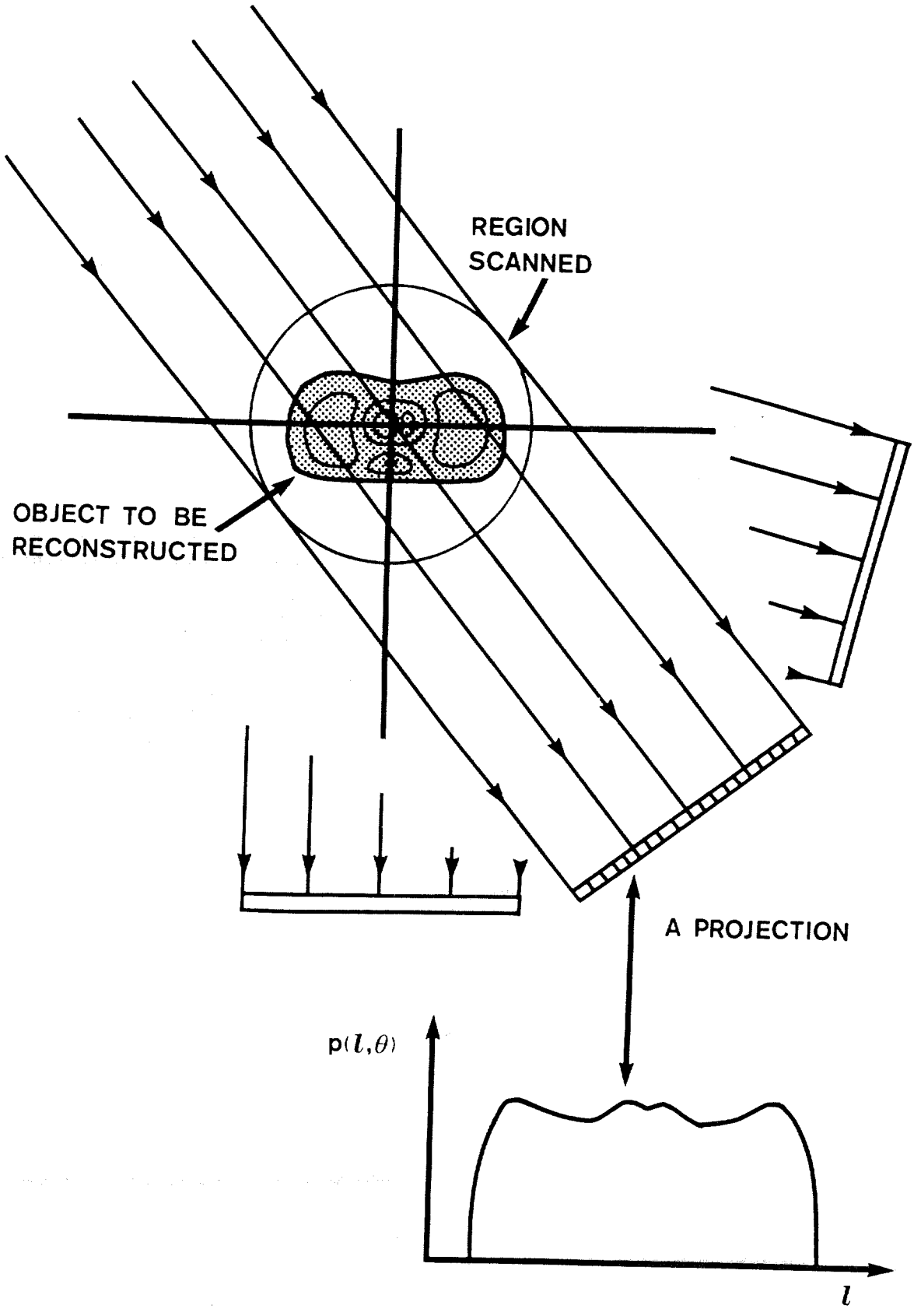
REGION
SCANNED
OBJECT TO BE
RECONSTRUCTED
A PROJECTION
p(l,θ)
l

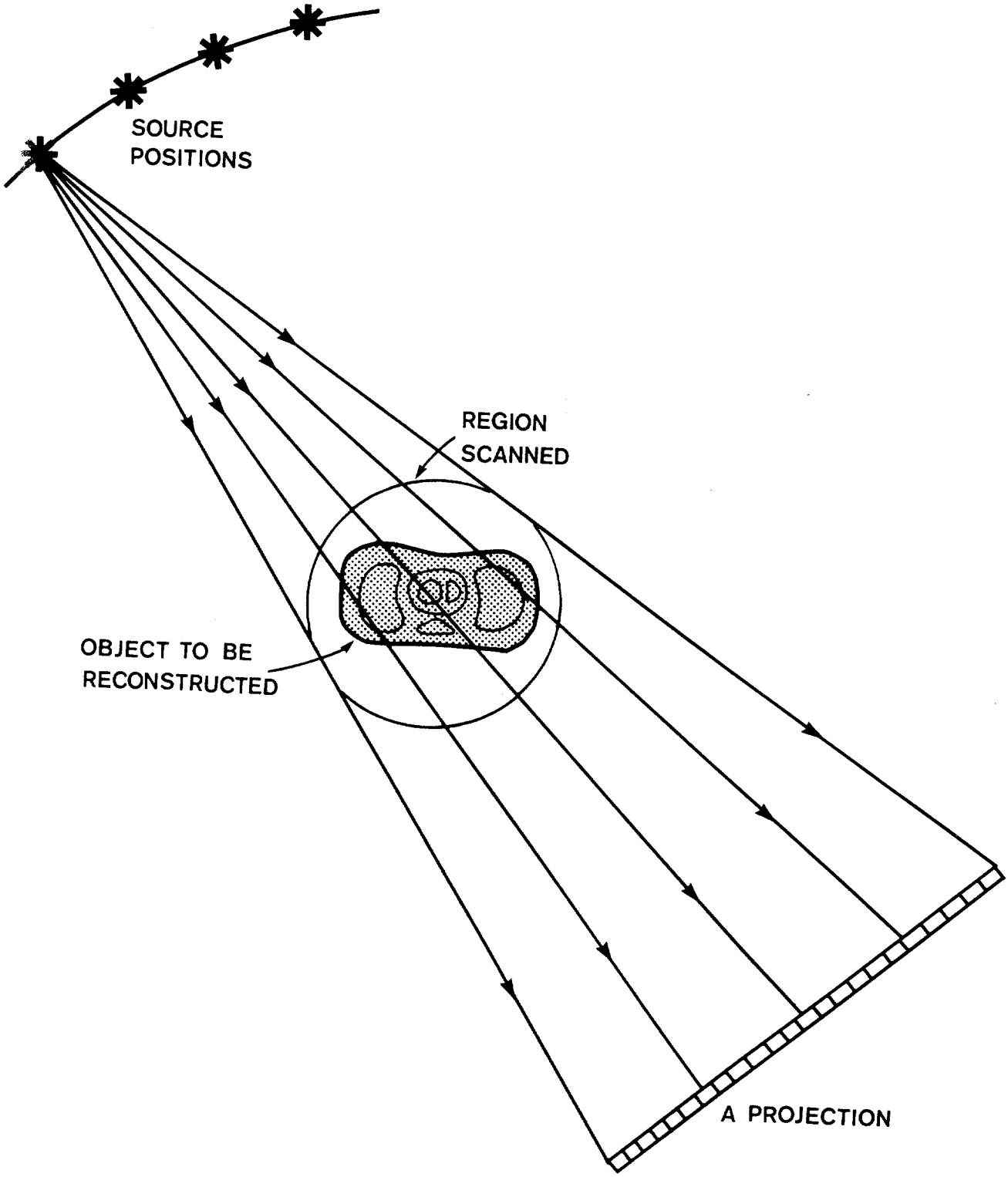
SOURCE
POSITIONS
REGION
SCANNED
OBJECT TO BE
RECONSTRUCTED
A PROJECTION

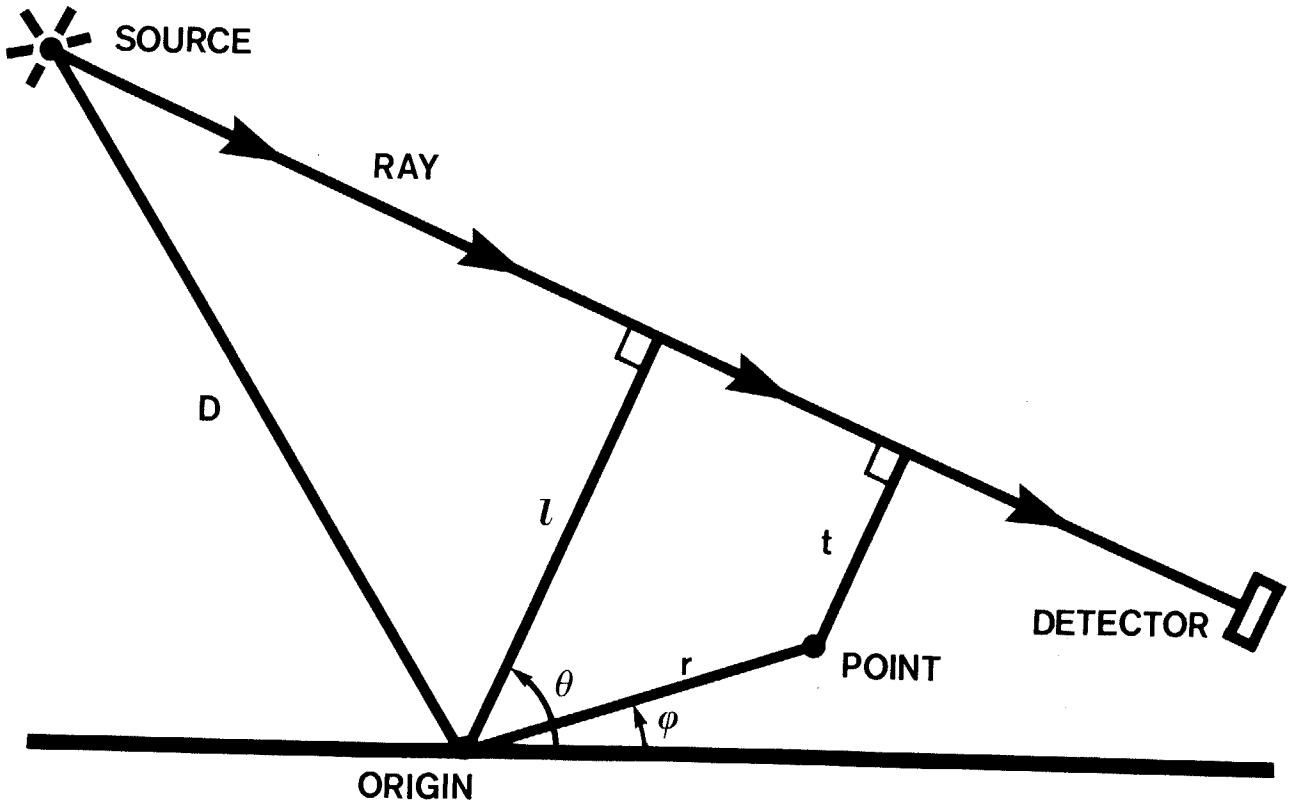
SOURCE
RAY
D
l
t
DETECTOR
POINT
r
θ
φ
ORIGIN

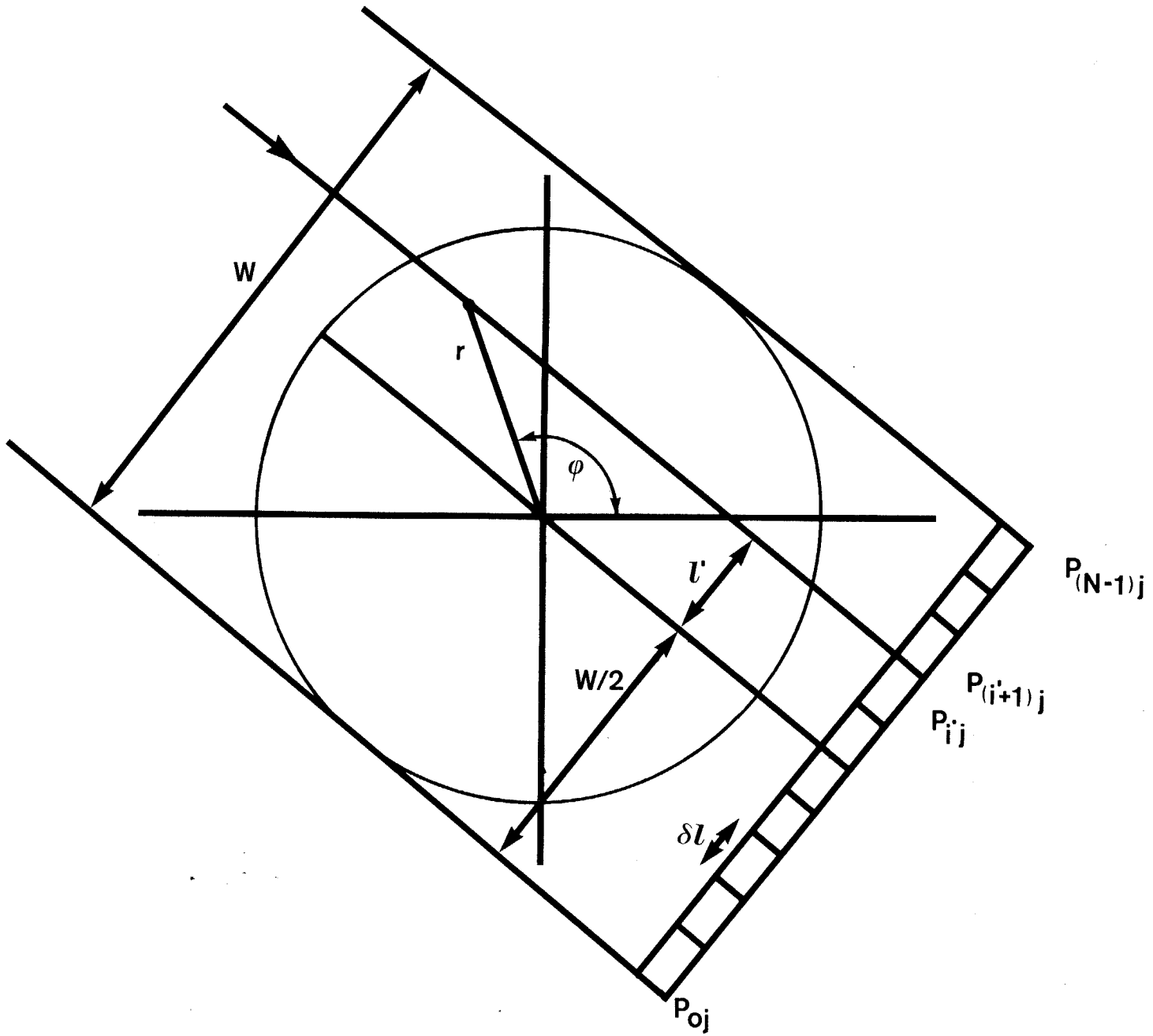
W
r
φ
l'
W/2
δl
P(N-1)j
P(i'+1)j
Pi'j
Poj

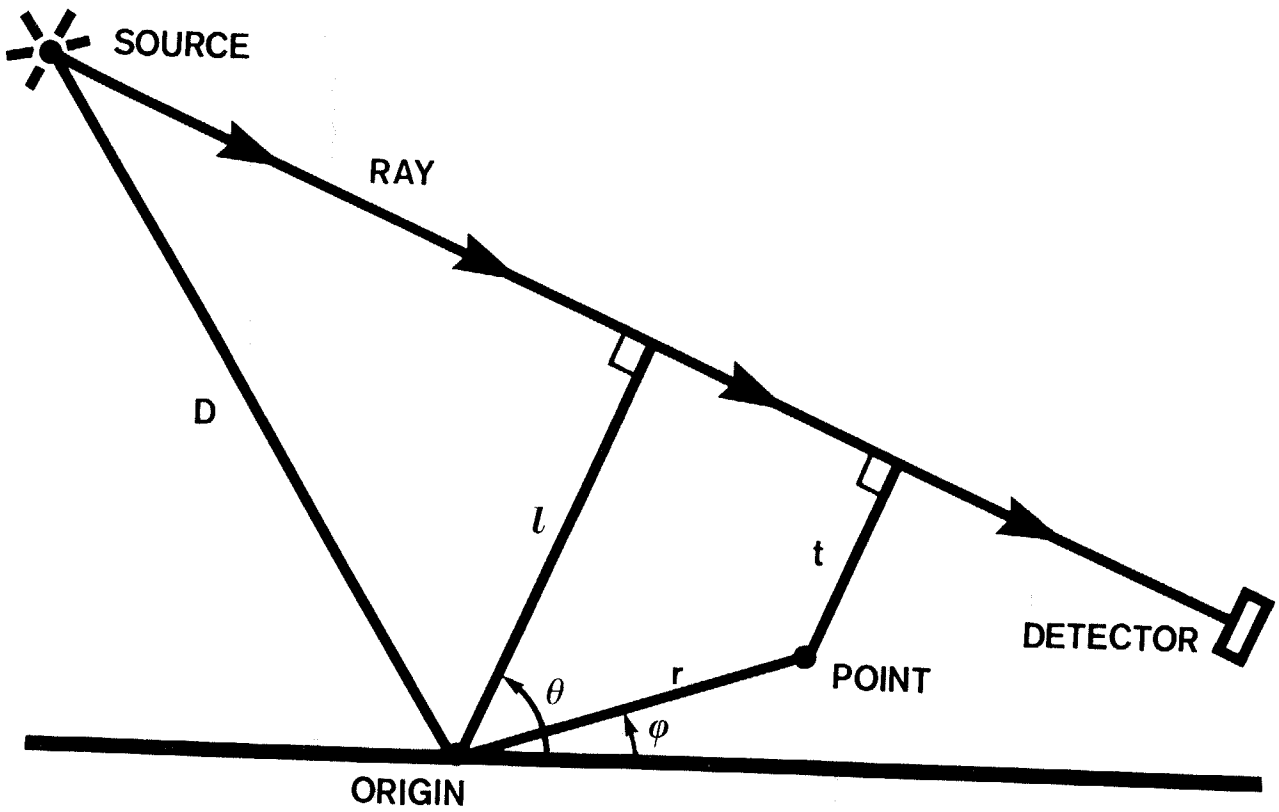
SOURCE
RAY
D
l
t
DETECTOR
θ
r
POINT
φ
ORIGIN

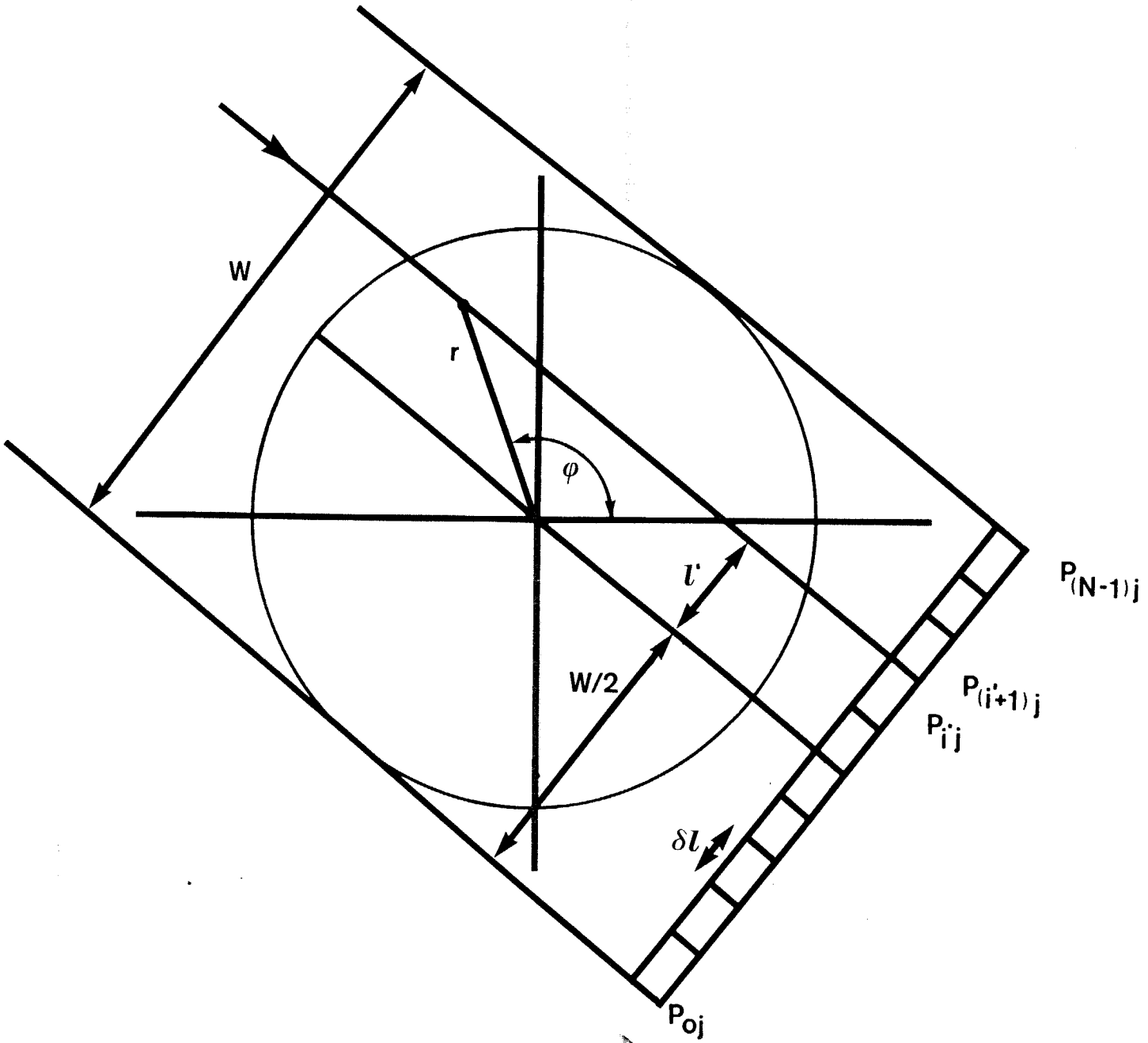
W
r
φ
l'
W/2
δl
P(N-1)j
P(i'+1)j
Pi'j
Poj

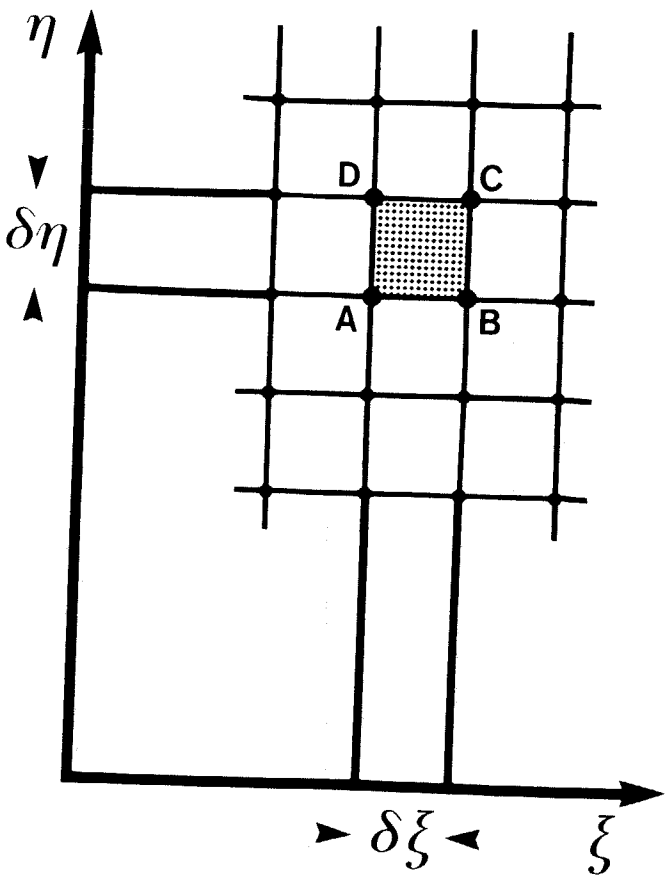
η
δη
D
C
A
B
δξ
ξ

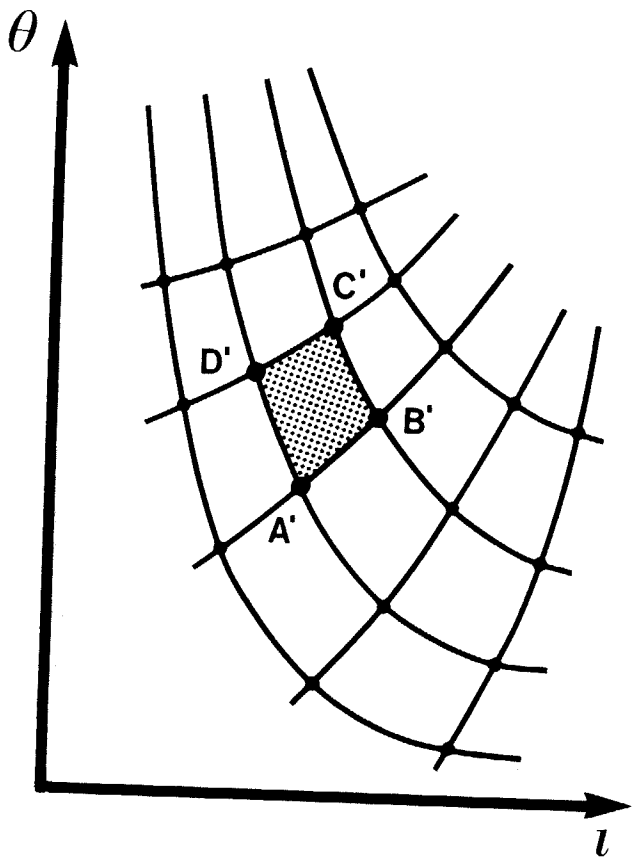
θ
C'
D'
B'
A'
ι

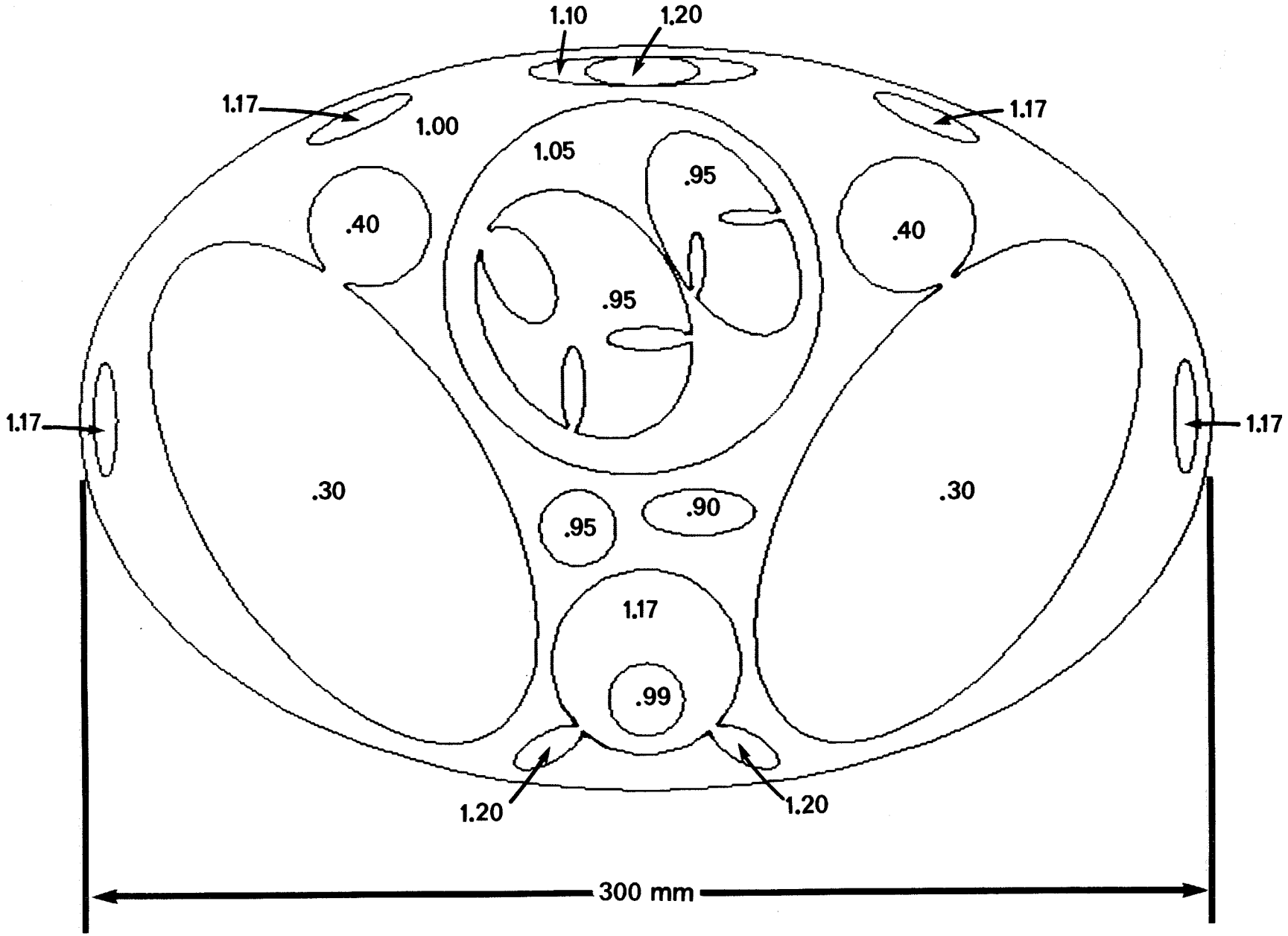
1.10
1.20
1.17
1.00
1.05
.95
1.17
.40
.40
.95
1.17
1.17
.30
.30
.95
.90
1.17
.99
1.20
1.20
300 mm

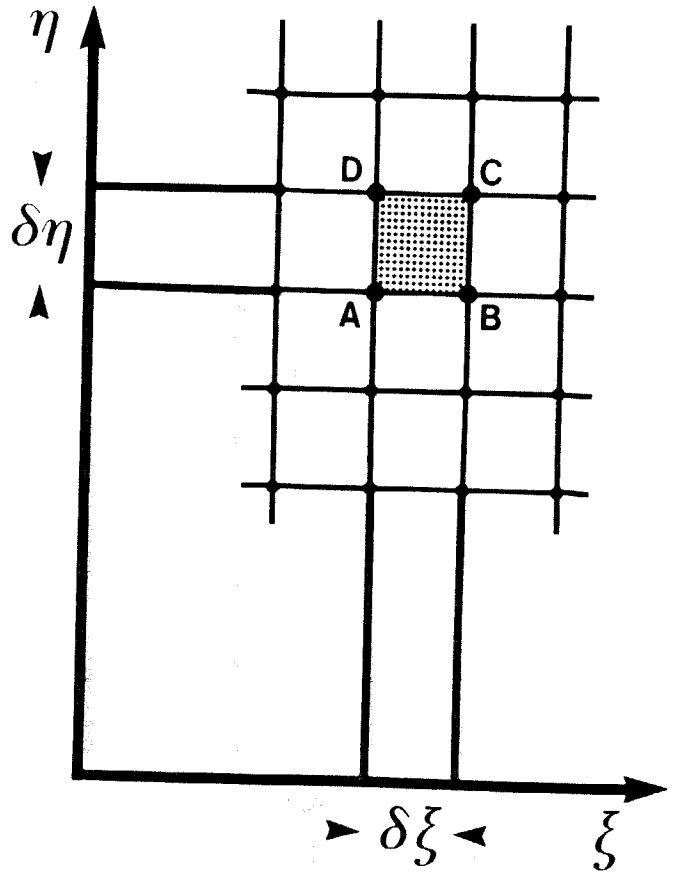
η
δη
D
C
A
B
δξ
ξ

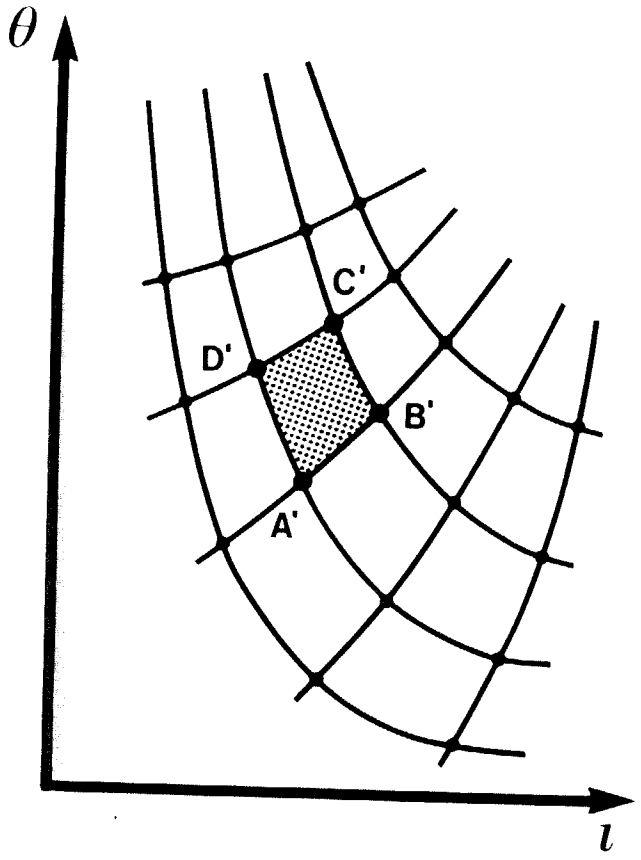
θ
C'
D'
B'
A'
ι

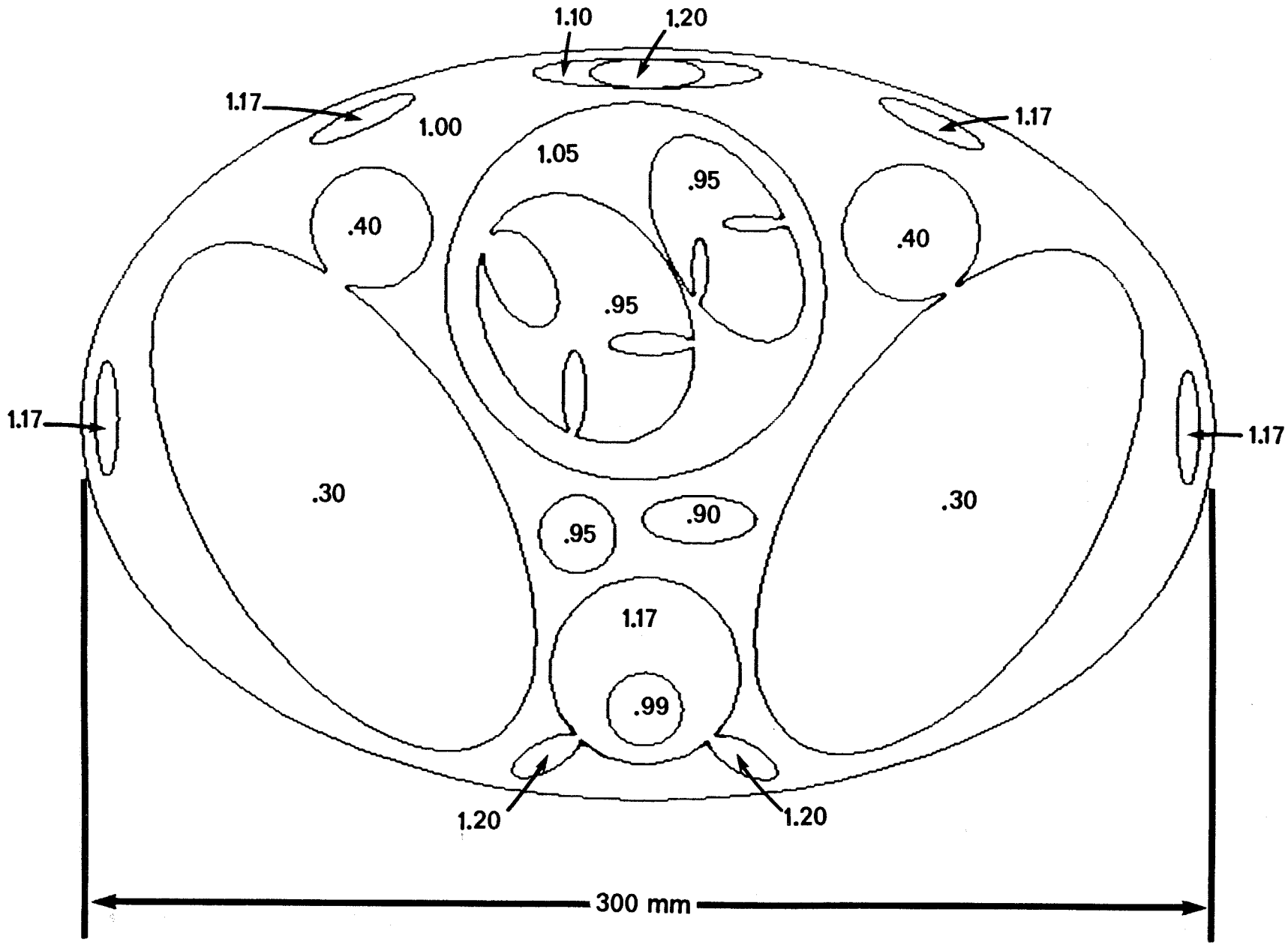
1.10
1.20
1.17
1.00
1.17
1.05
.95
.40
.40
.95
1.17
1.17
.30
.30
.95
.90
1.17
.99
1.20
1.20
300 mm

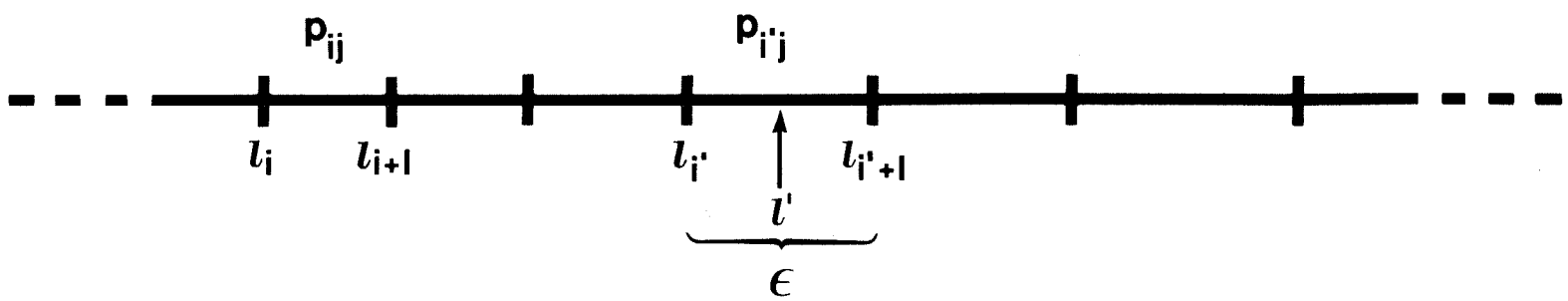
p_{ij}
$p_{i'j}$
l_i
l_{i+1}
$l_{i'}$
$l_{i'+1}$
l'
ϵ

220. 202. 151. 400.0 330.0 0.0 0.0

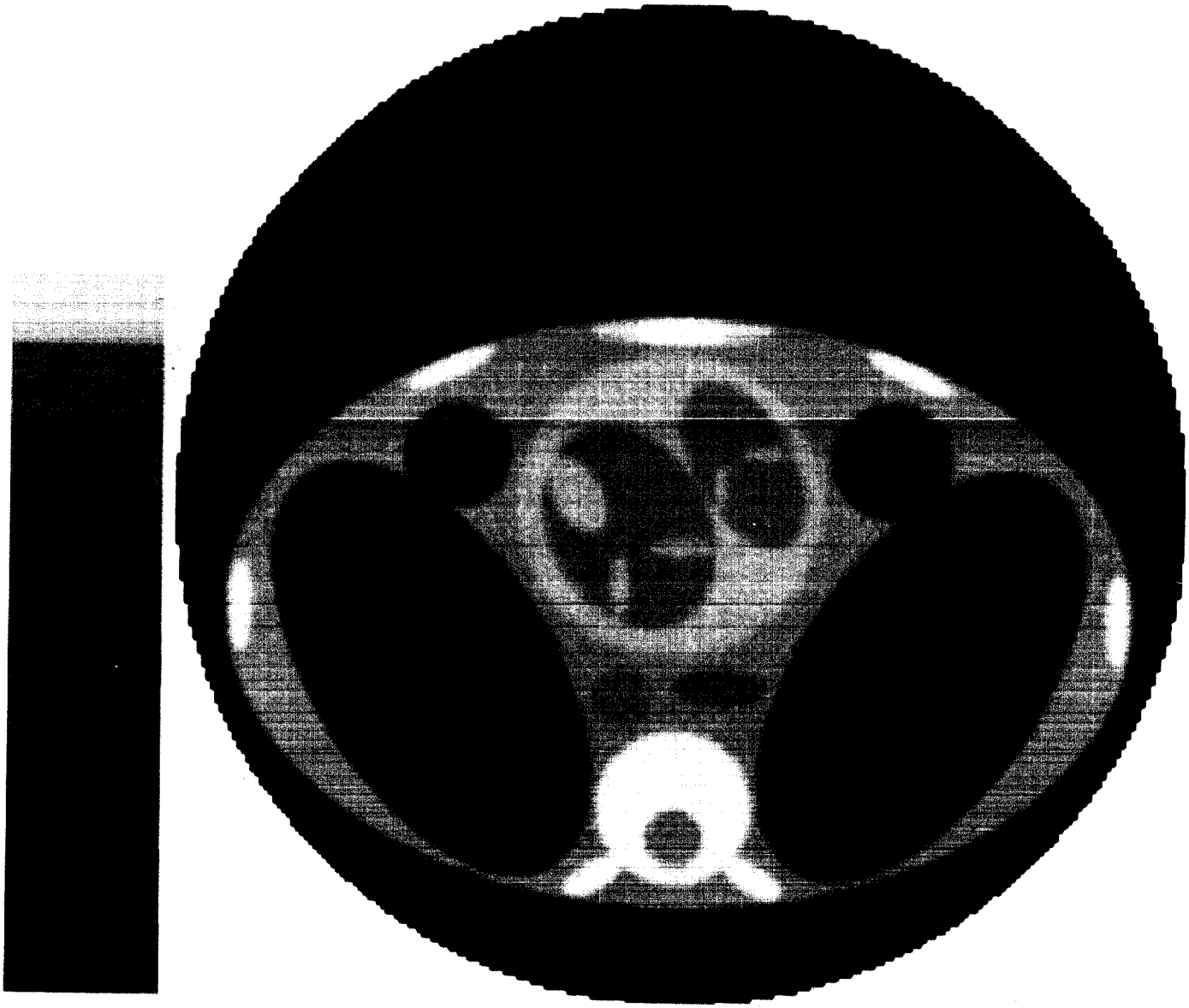

IMAGE1.1

8A

GA

Shadow Density 193

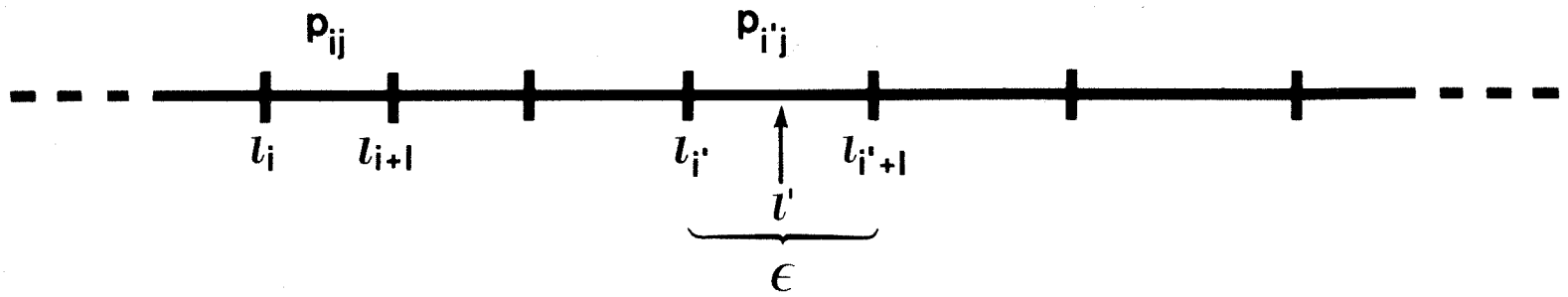
p_{ij}
$p_{i'j}$
l_i
l_{i+1}
$l_{i'}$
$l_{i'+1}$
l'
ϵ

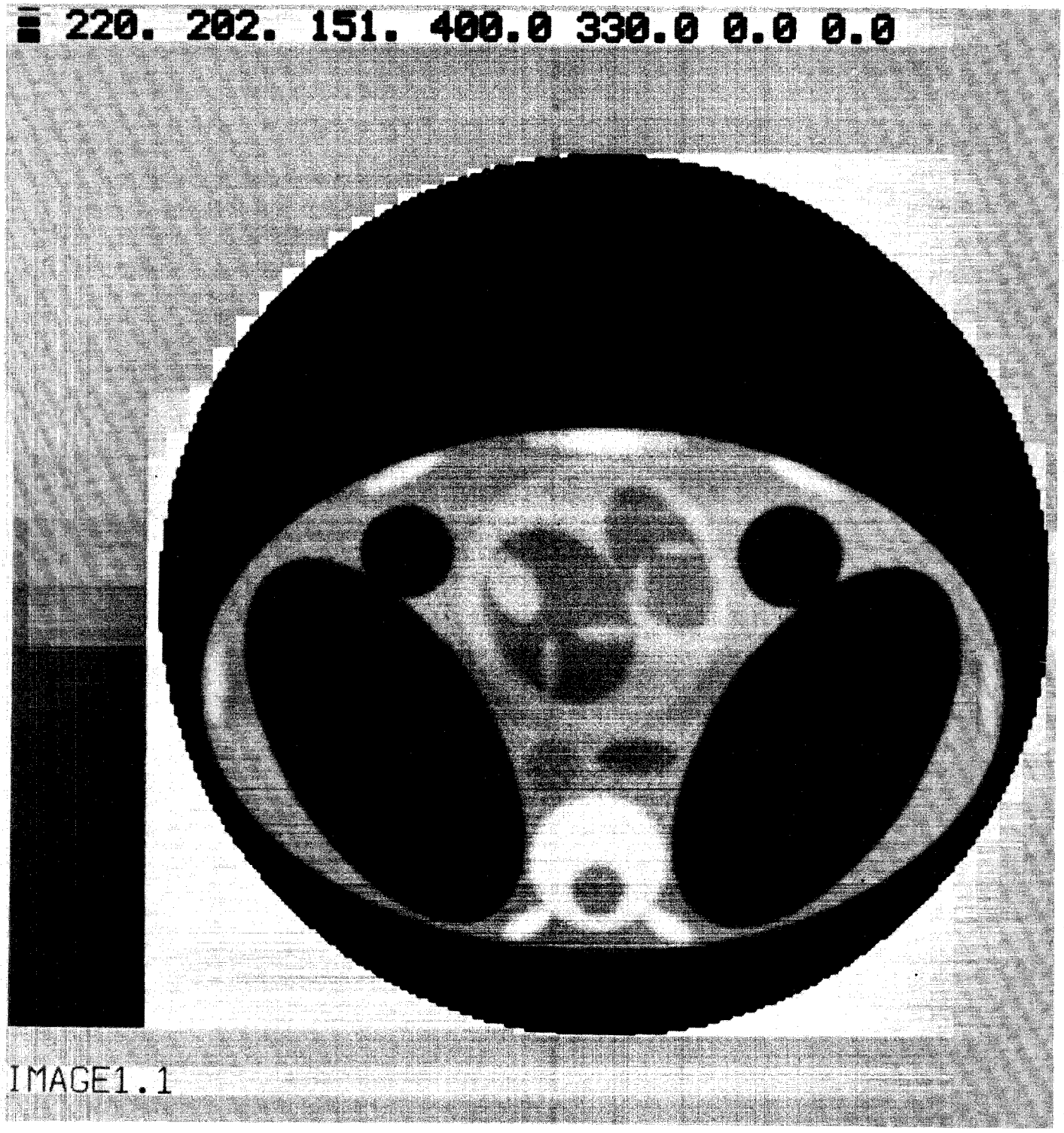
220. 202. 151. 400.0 330.0 0.0 0.0
IMAGE1.1

220. 102. 151. 400.0 330.0 0.5 0.0

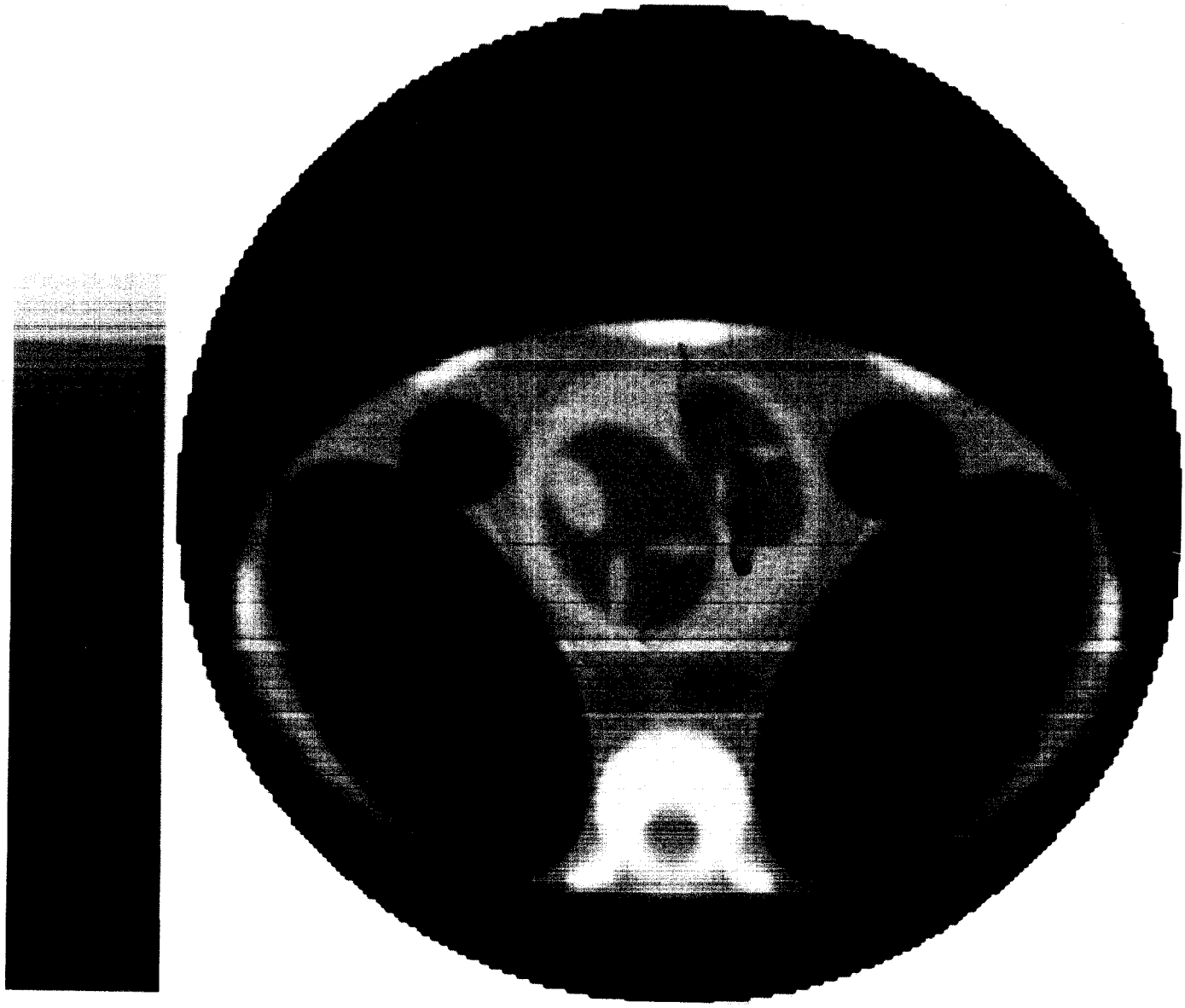

IMAGE1.3

8B

GA

Shadow Density 190

≡ 220. 102. 151. 400.0 330.0 0.0 0.0

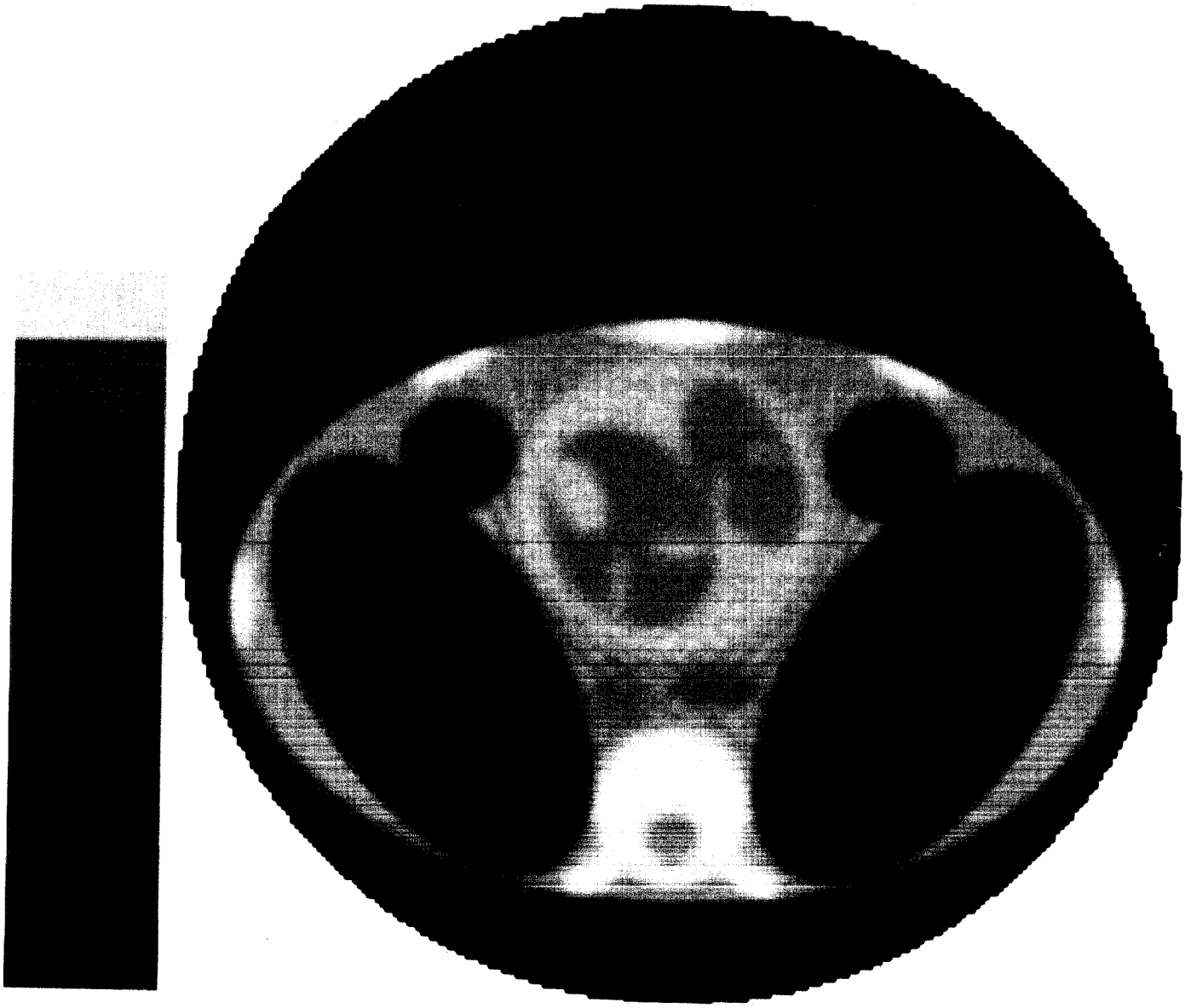

IMAGE1.5

8C

GA

Shadow Density 192

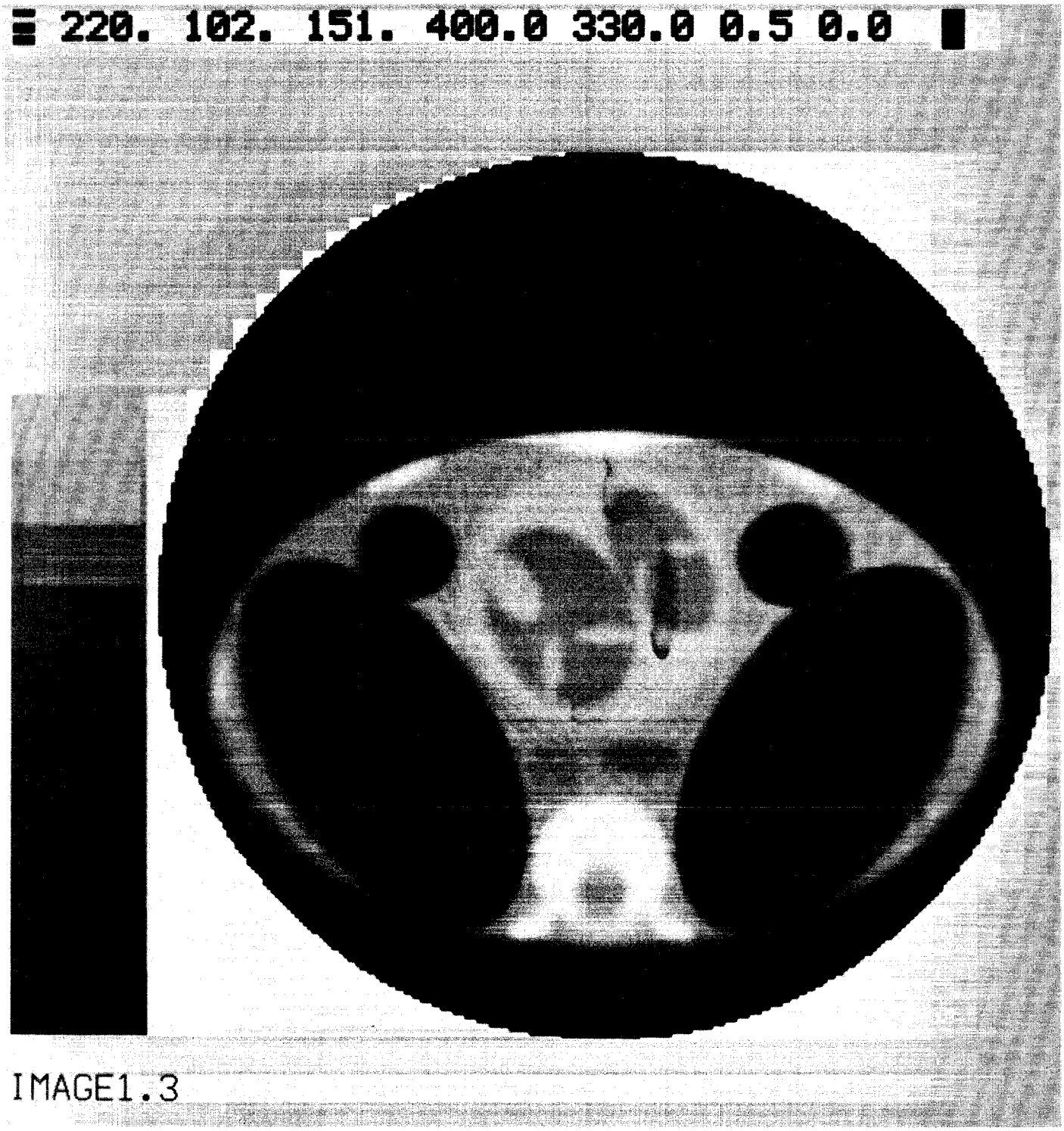
220. 102. 151. 400.0 330.0 0.5 0.0
IMAGE1.3

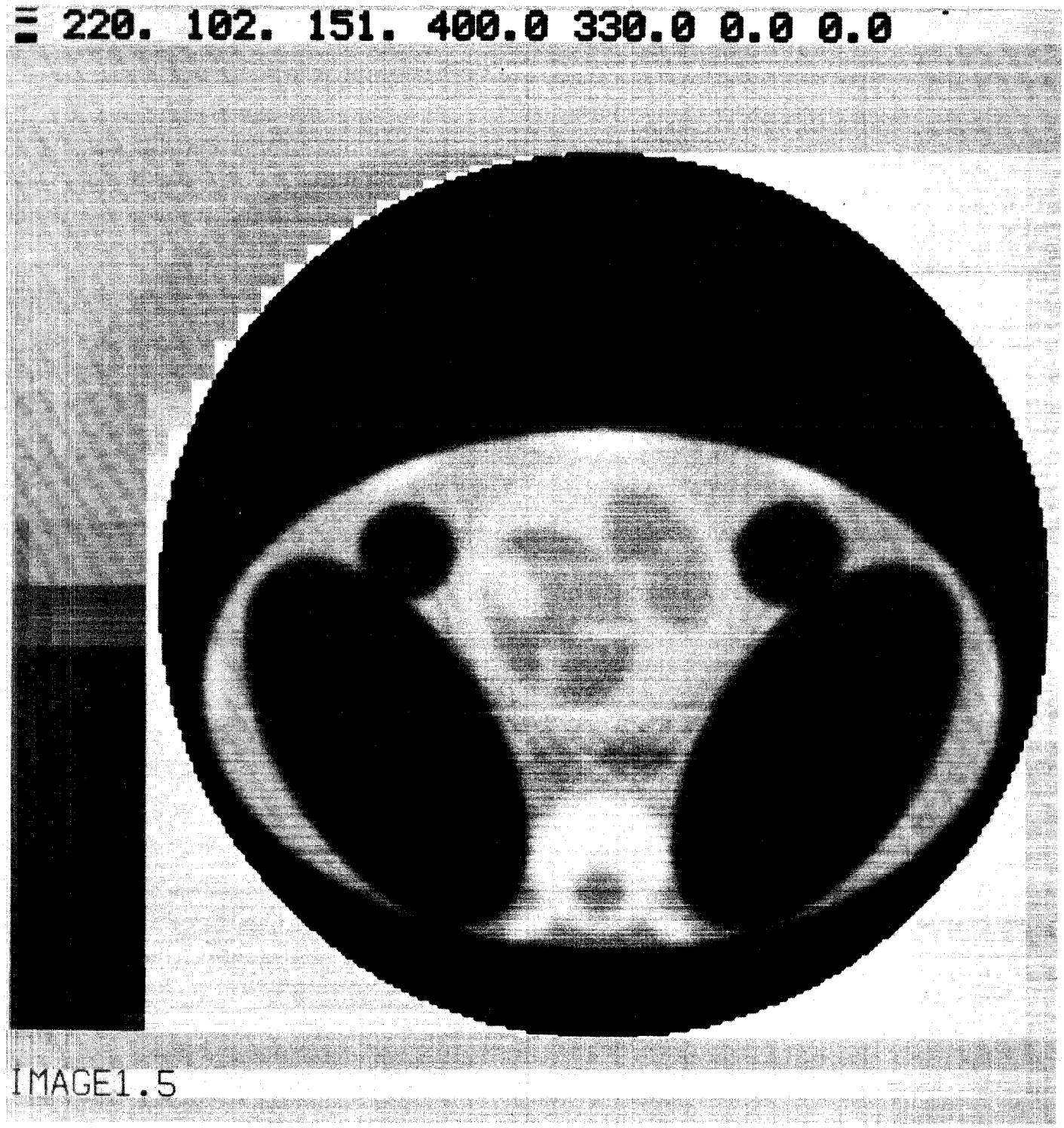
220. 102. 151. 400.0 330.0 0.0 0.0
IMAGE1.5

≡ 220. 202. 151. 400.0 330.0 0.0 0.0

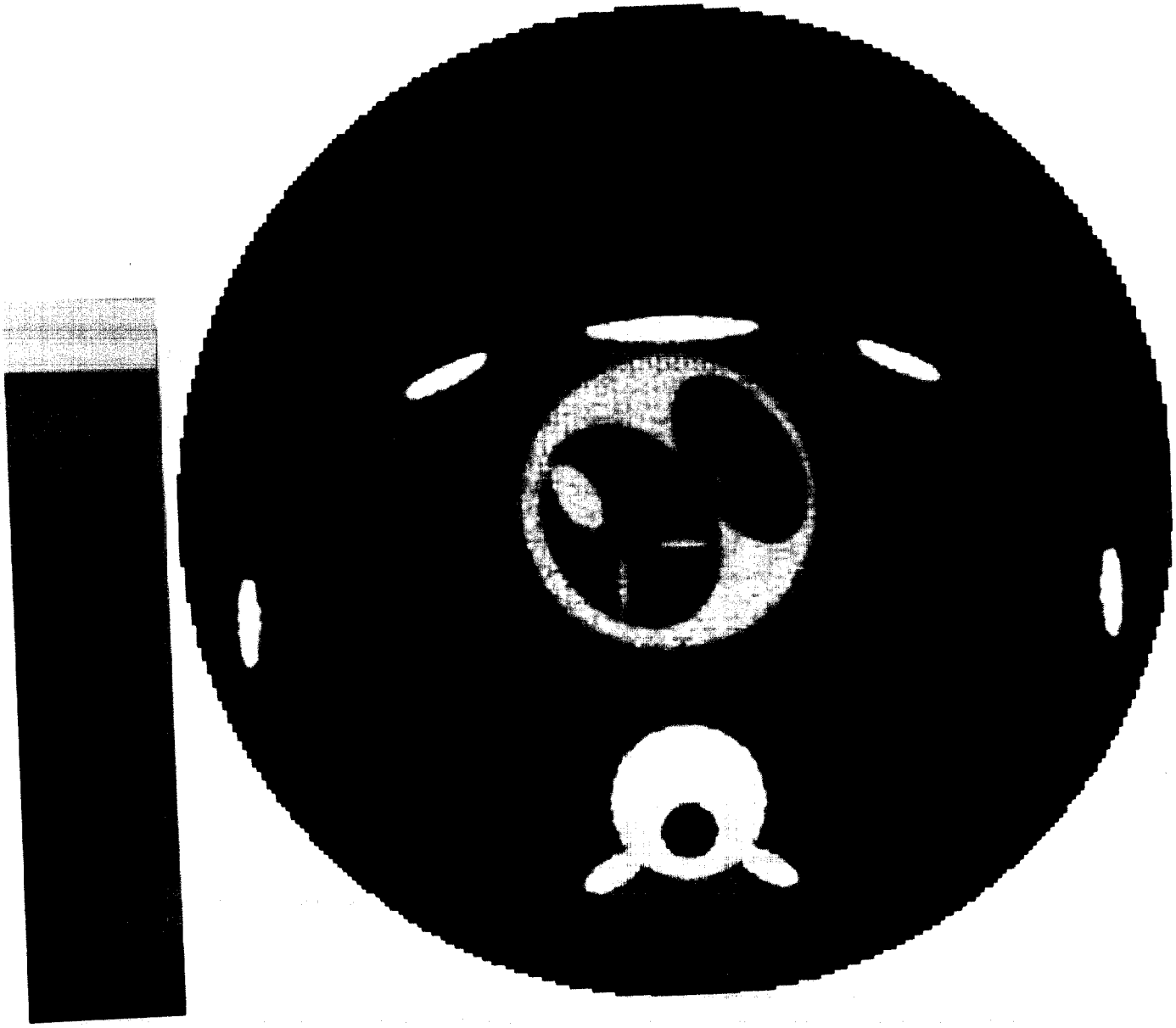

IMAGE1.2

94

GA

Shadow Density 194

220. 102. 151. 400.0 330.0 0.5 0.0

IMAGE1.4

9B

GA

Shadow Density 196

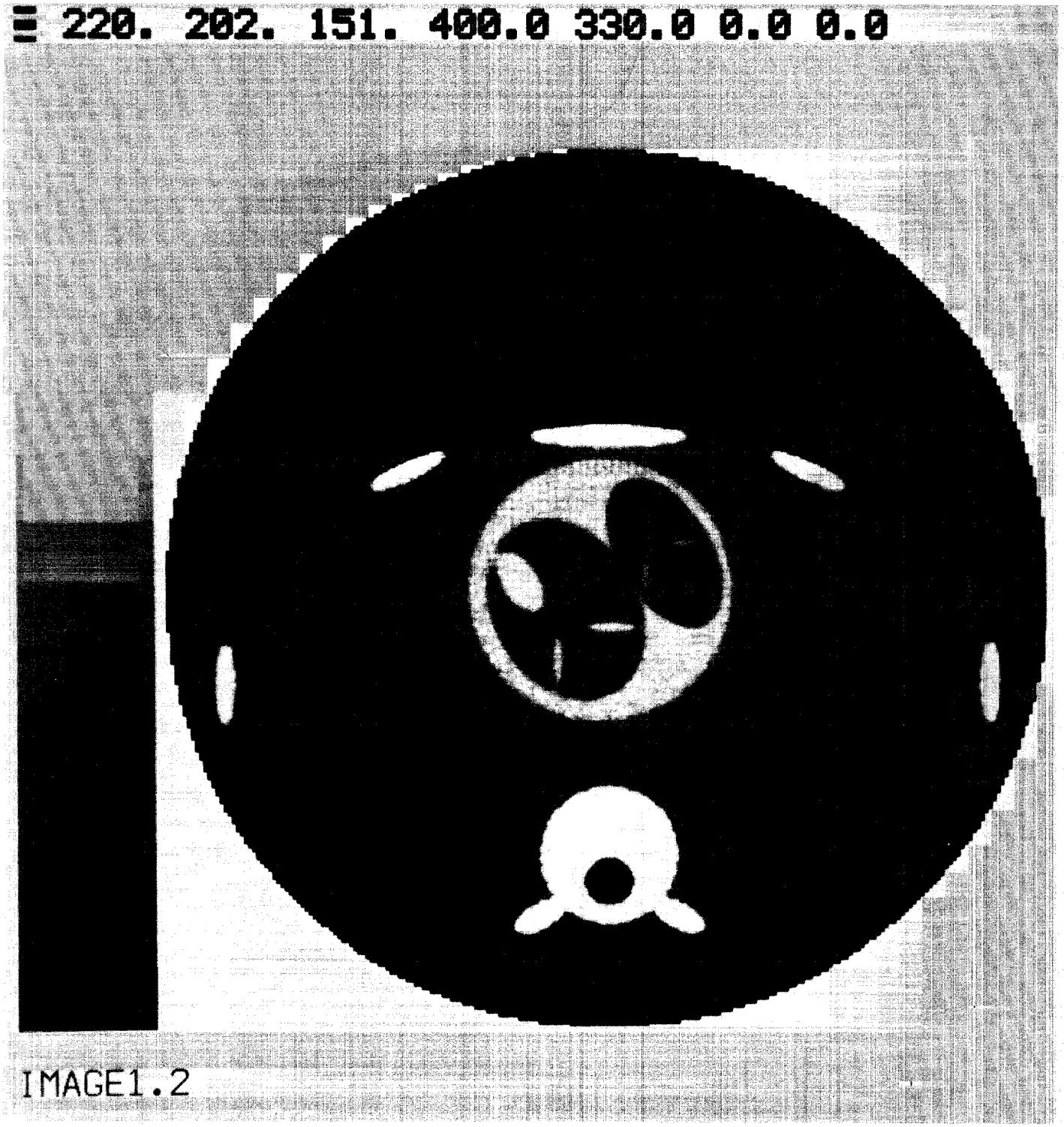
220. 202. 151. 400.0 330.0 0.0 0.0
IMAGE1.2

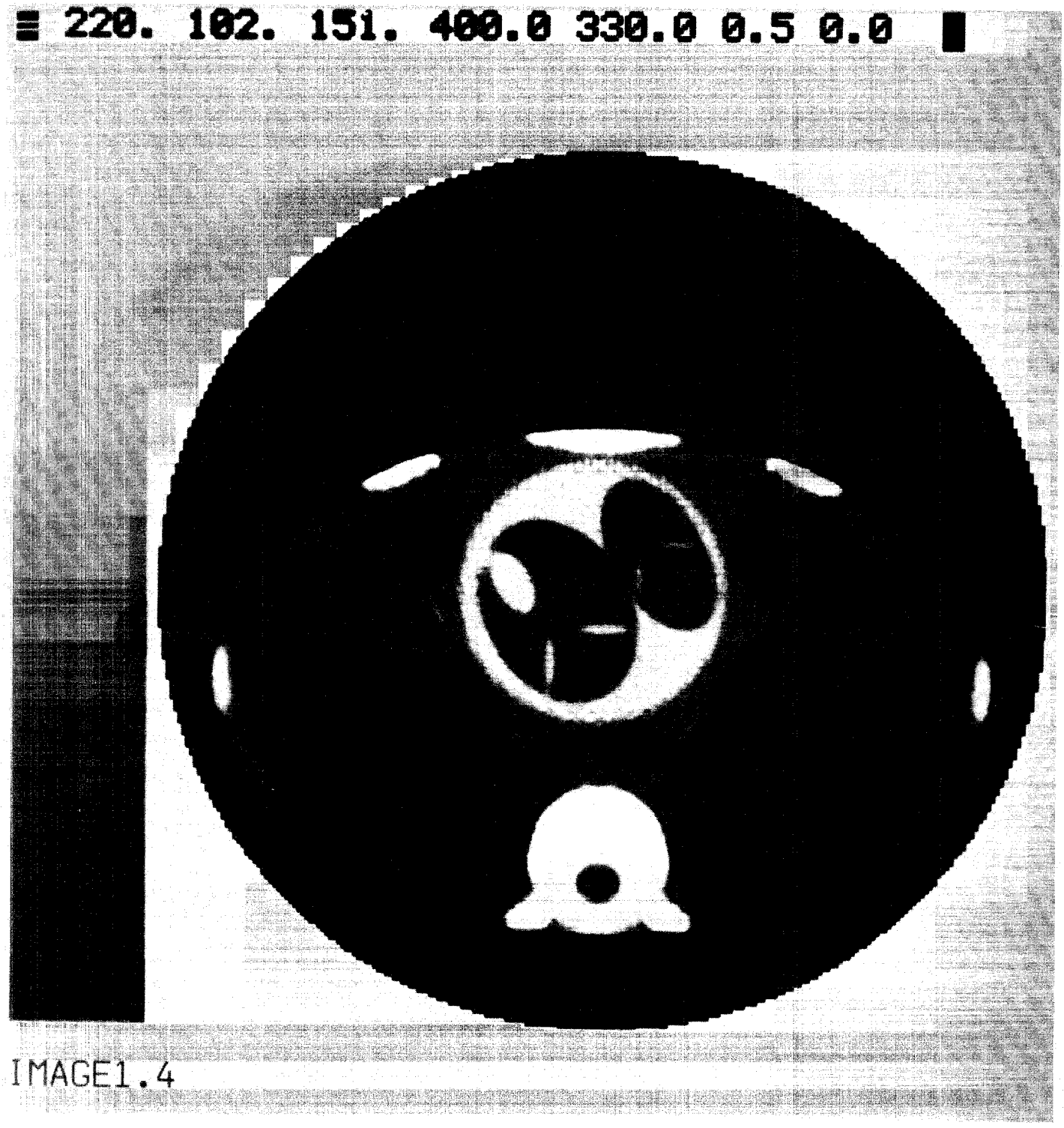
220. 102. 151. 400.0 330.0 0.5 0.0
IMAGE1.4

≦ 220. 102. 151. 400.0 330.0 0.0 0.0 ▮

IMAGE1.6

9C

GA

Shadow Density 197

200. 202. 151. 400.0 150.0 0.0 0.0

IMAGE1.7

10A

GA

Shadow Density 188

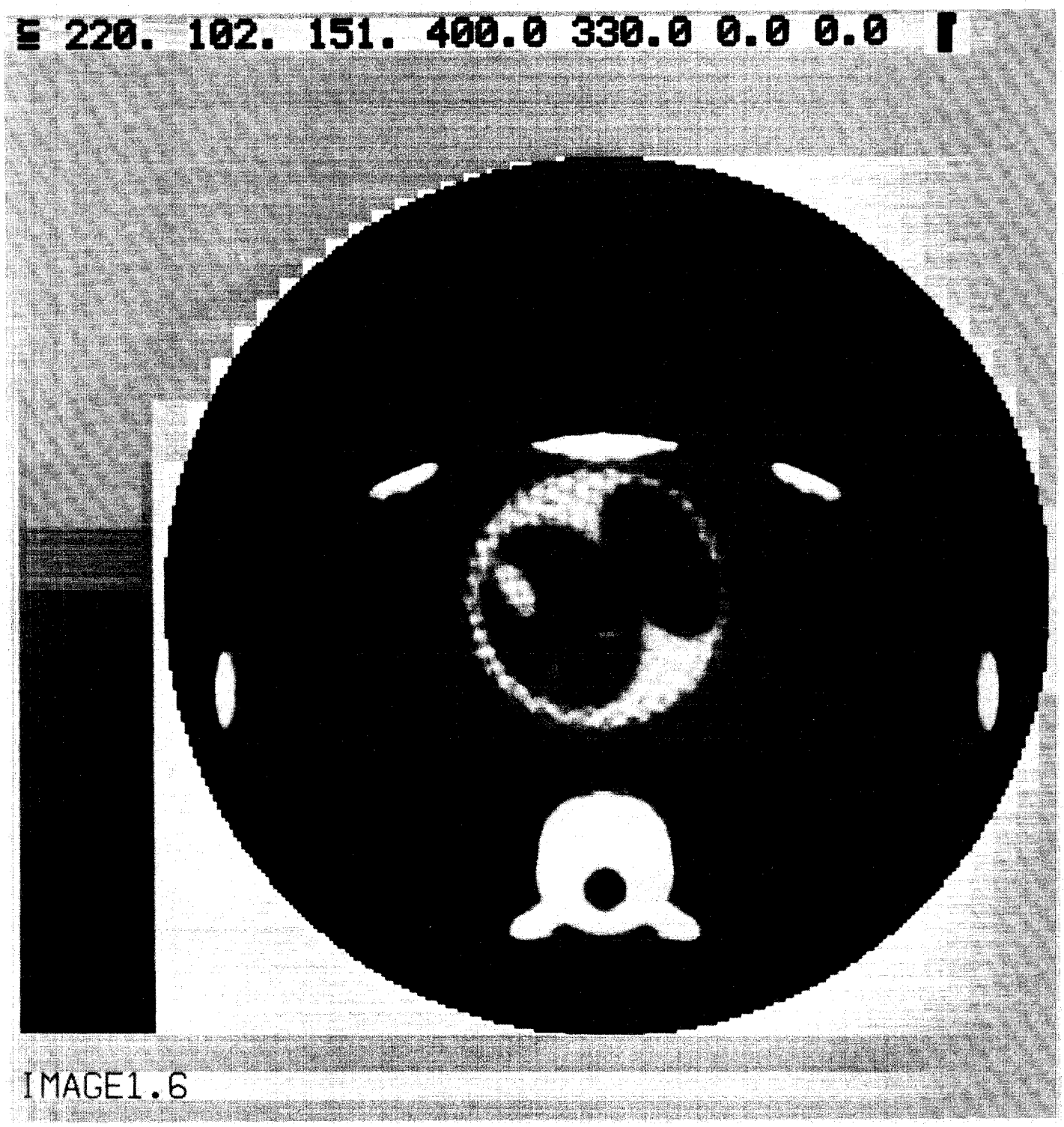
≦ 220. 102. 151. 400.0 330.0 0.0 0.0
IMAGE1.6

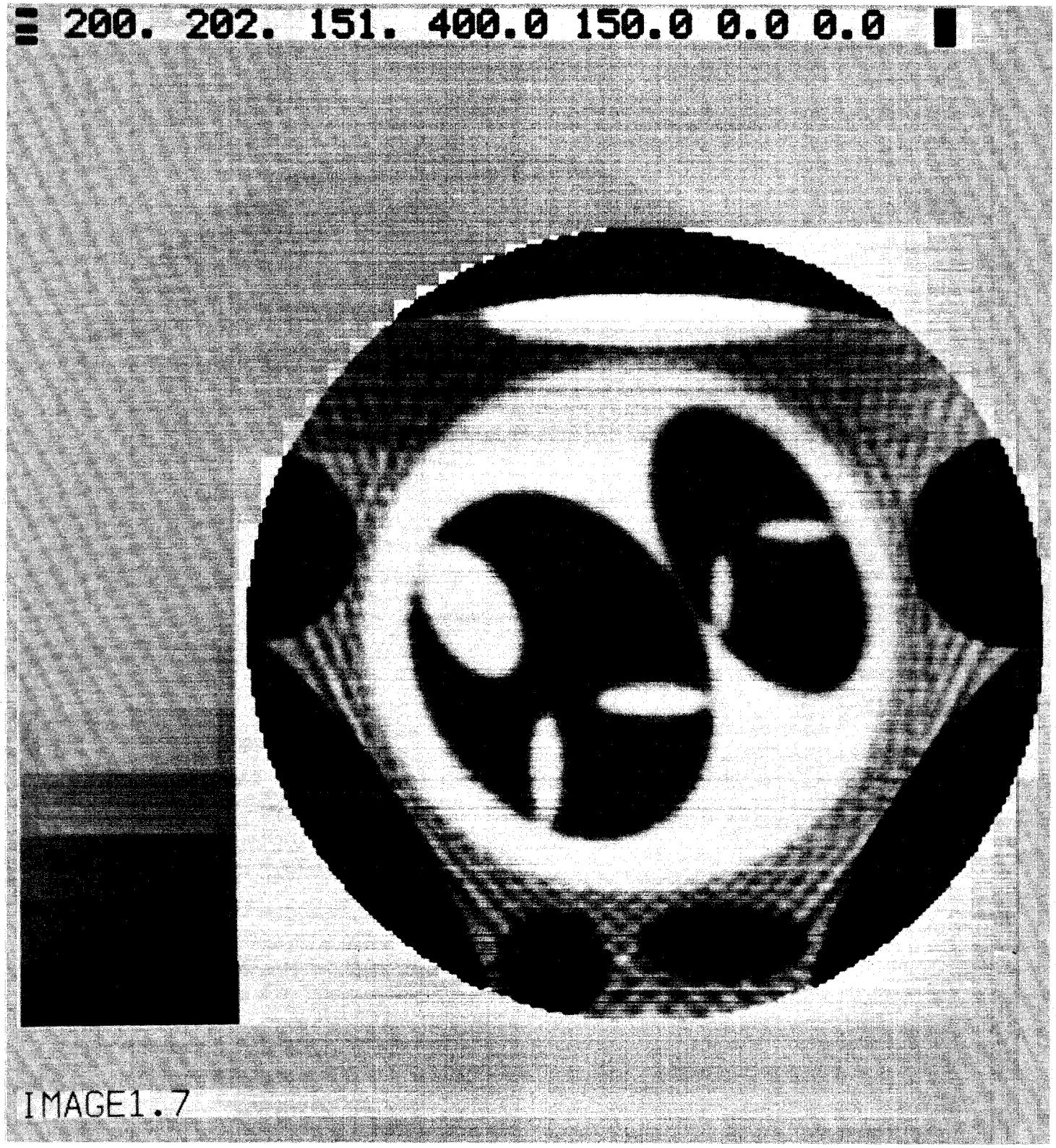
200. 202. 151. 400.0 150.0 0.0 0.0
IMAGE1.7

200. 102. 151. 400.0 150.0 0.5 0.0

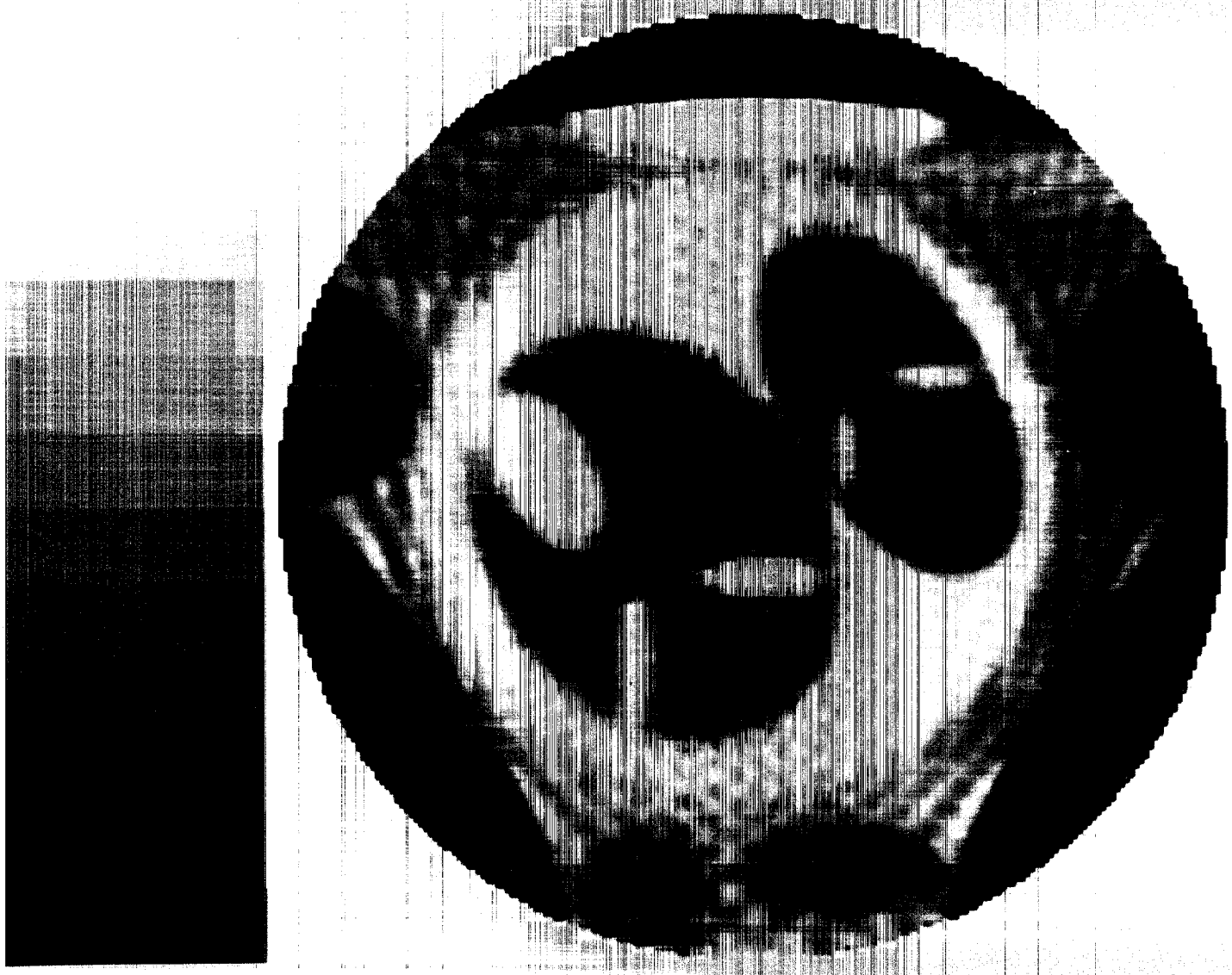

IMAGE1.8

10B

GA

Shadow Density 201

≡ 200. 102. 151. 400.0 150.0 0.0 0.0

IMAGE1.9

10C

GA

Shadow Density 193

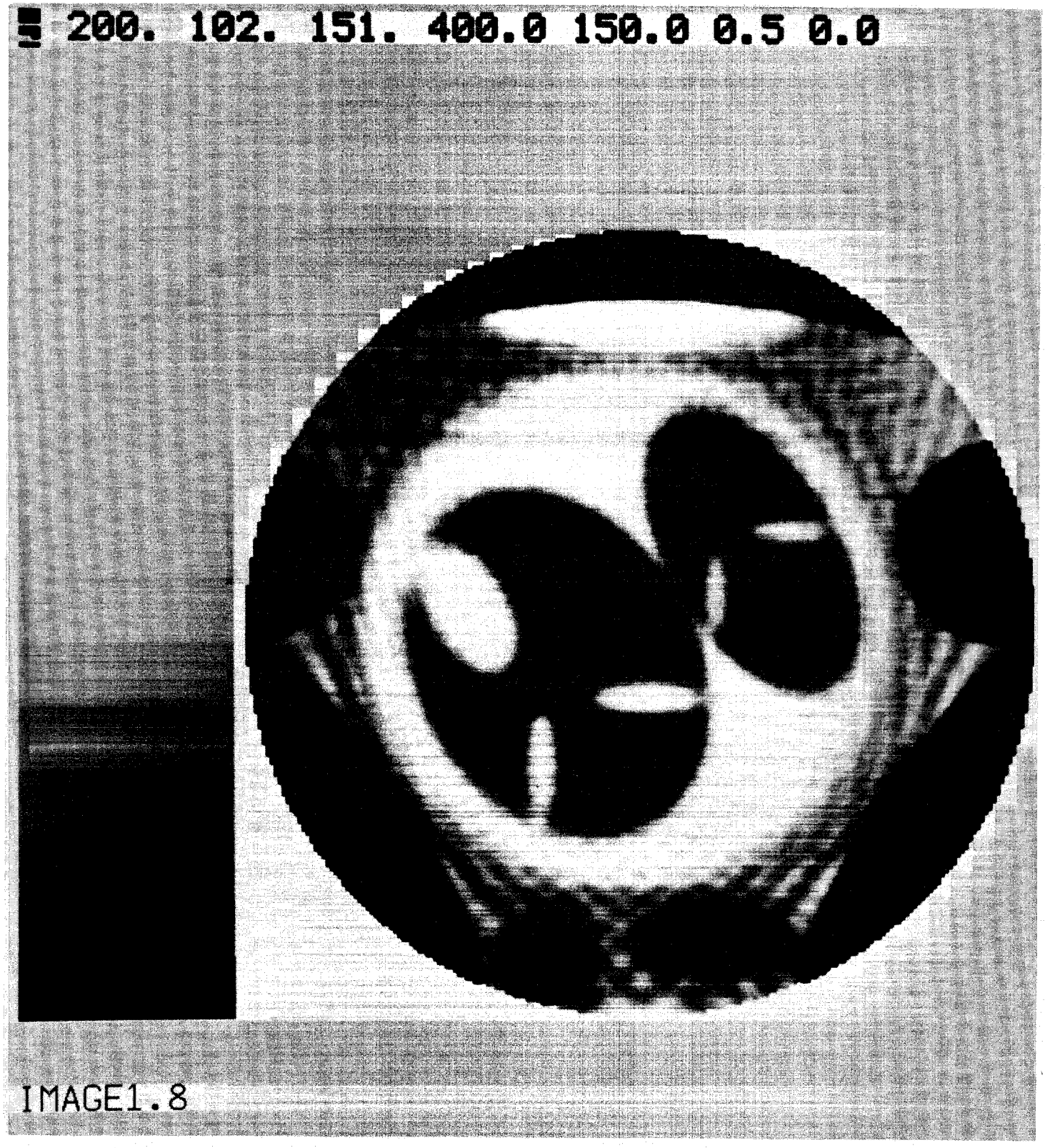
200. 102. 151. 400.0 150.0 0.5 0.0
IMAGE1.8

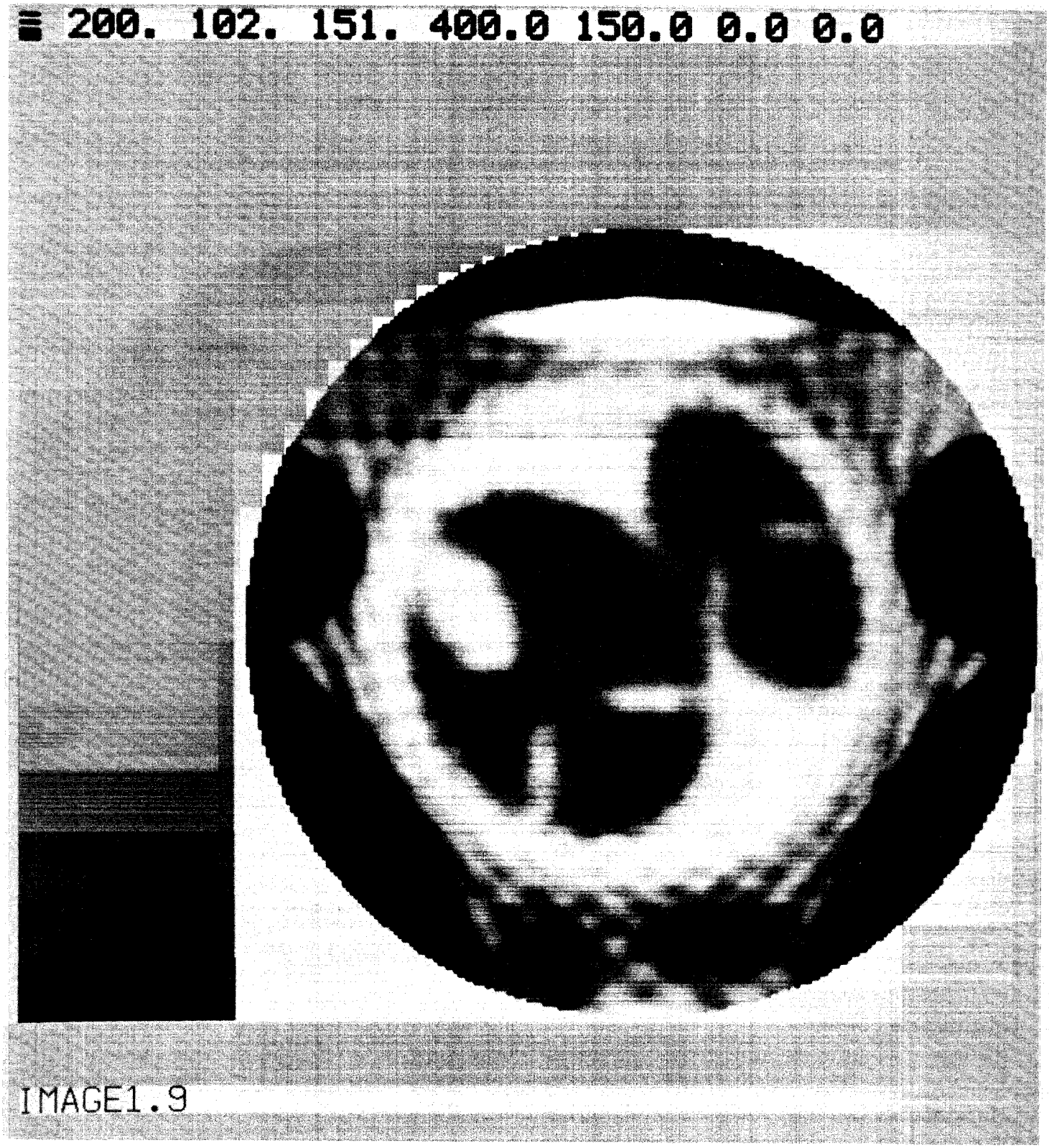
200. 102. 151. 400.0 150.0 0.0 0.0
IMAGE1.9

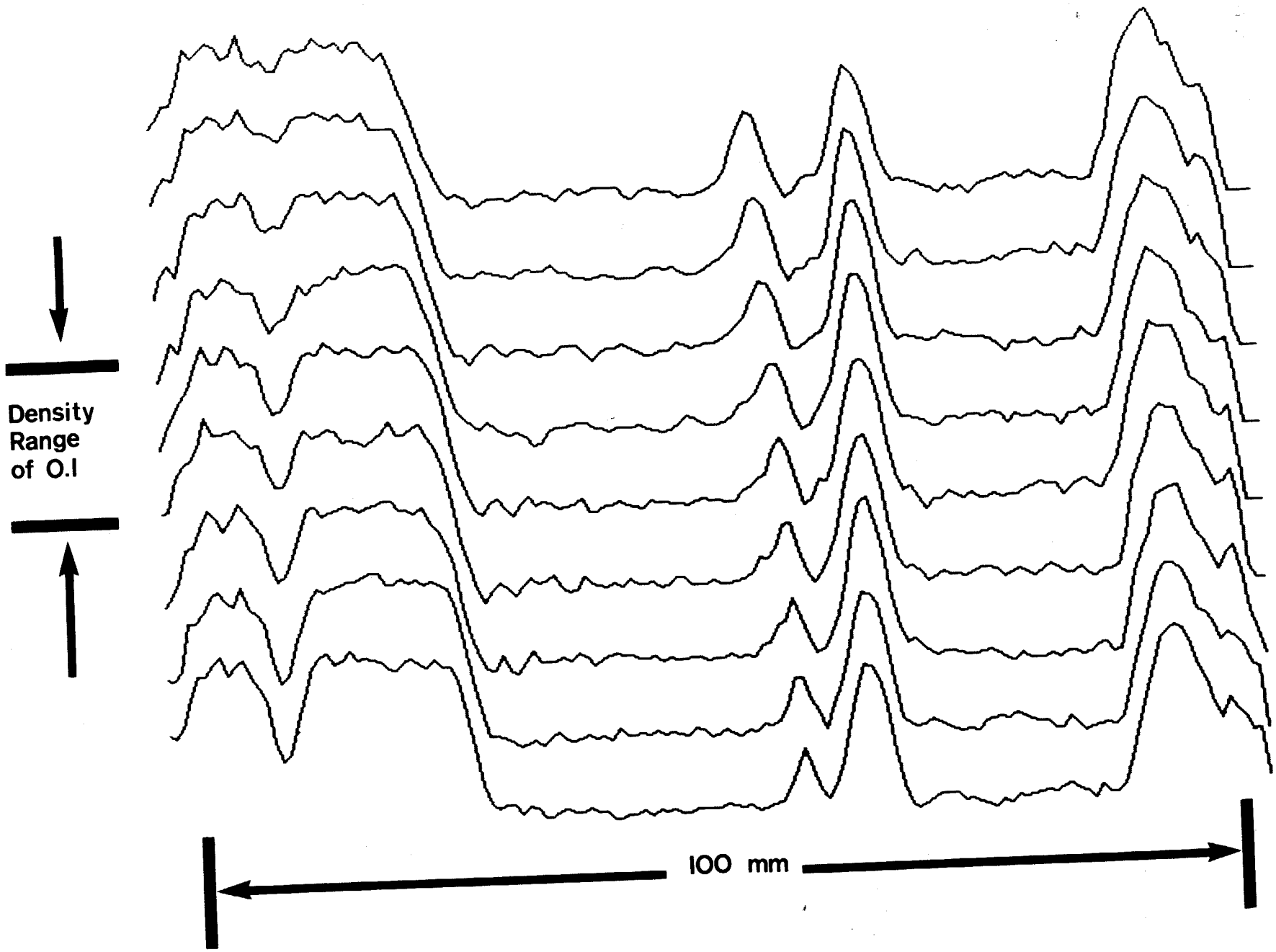
Density
Range
of O.I
100 mm

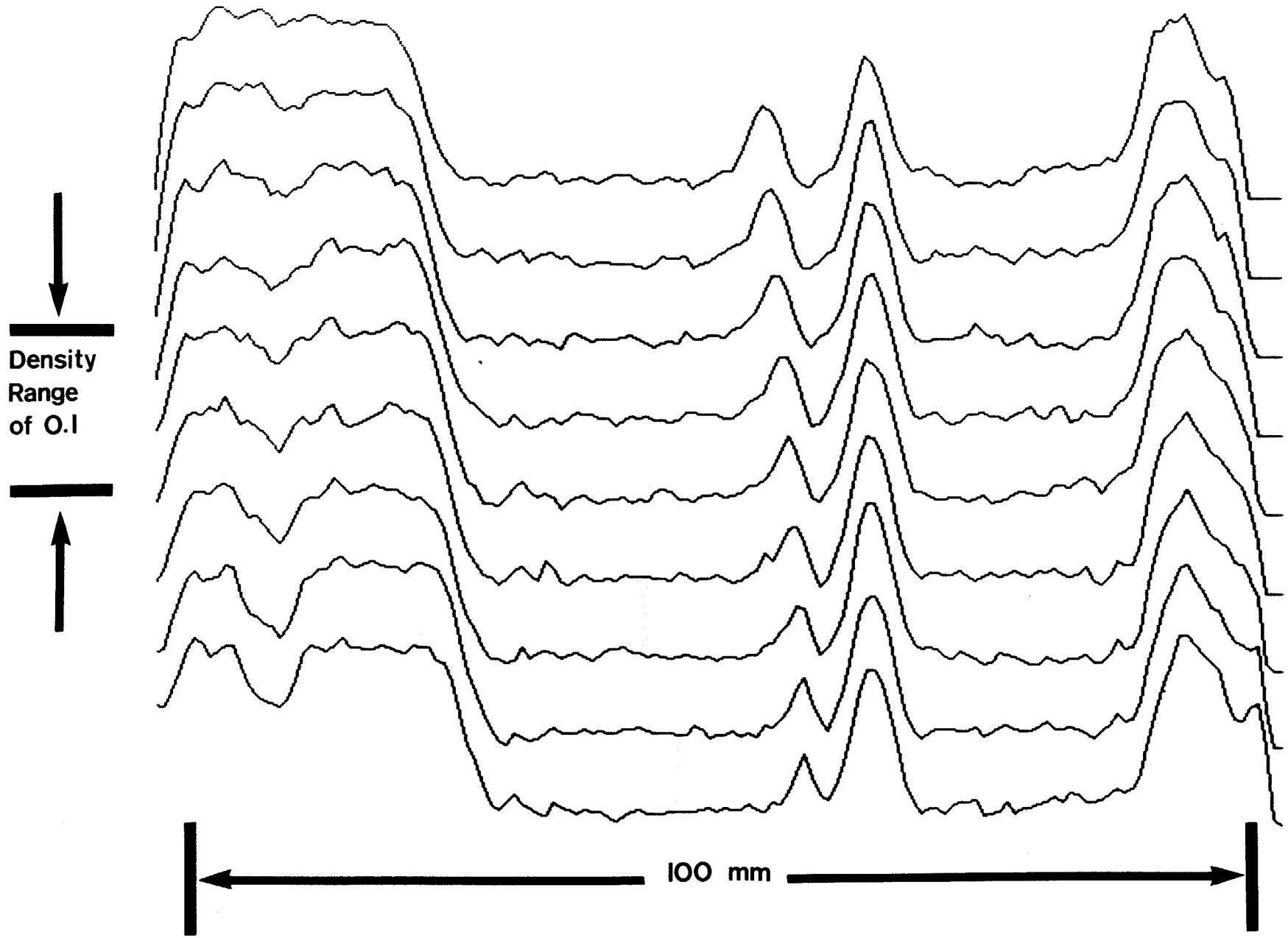
Density
Range
of O.I
100 mm

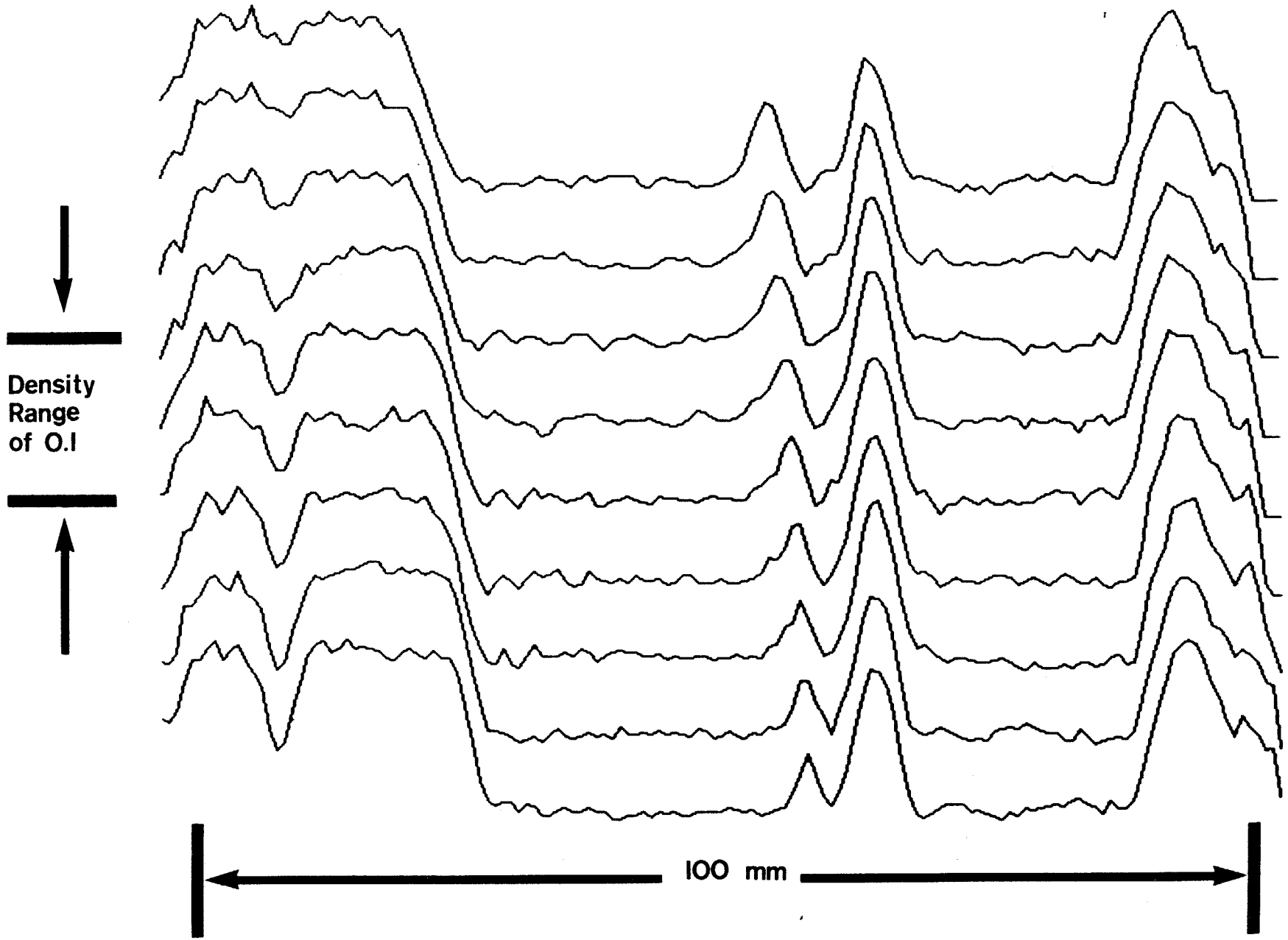
Density
Range
of O.I
100 mm

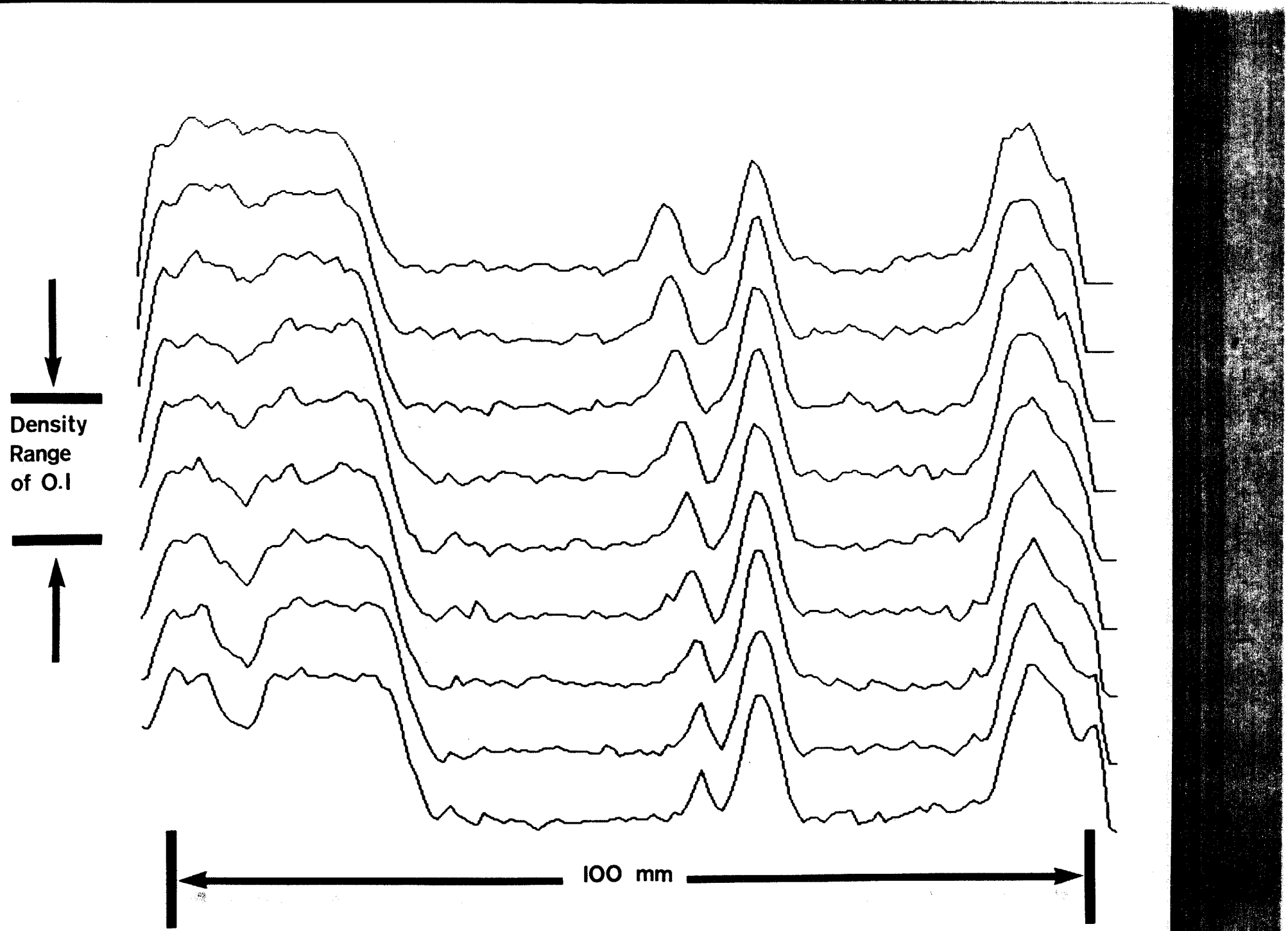
Density
Range
of 0.1
100 mm

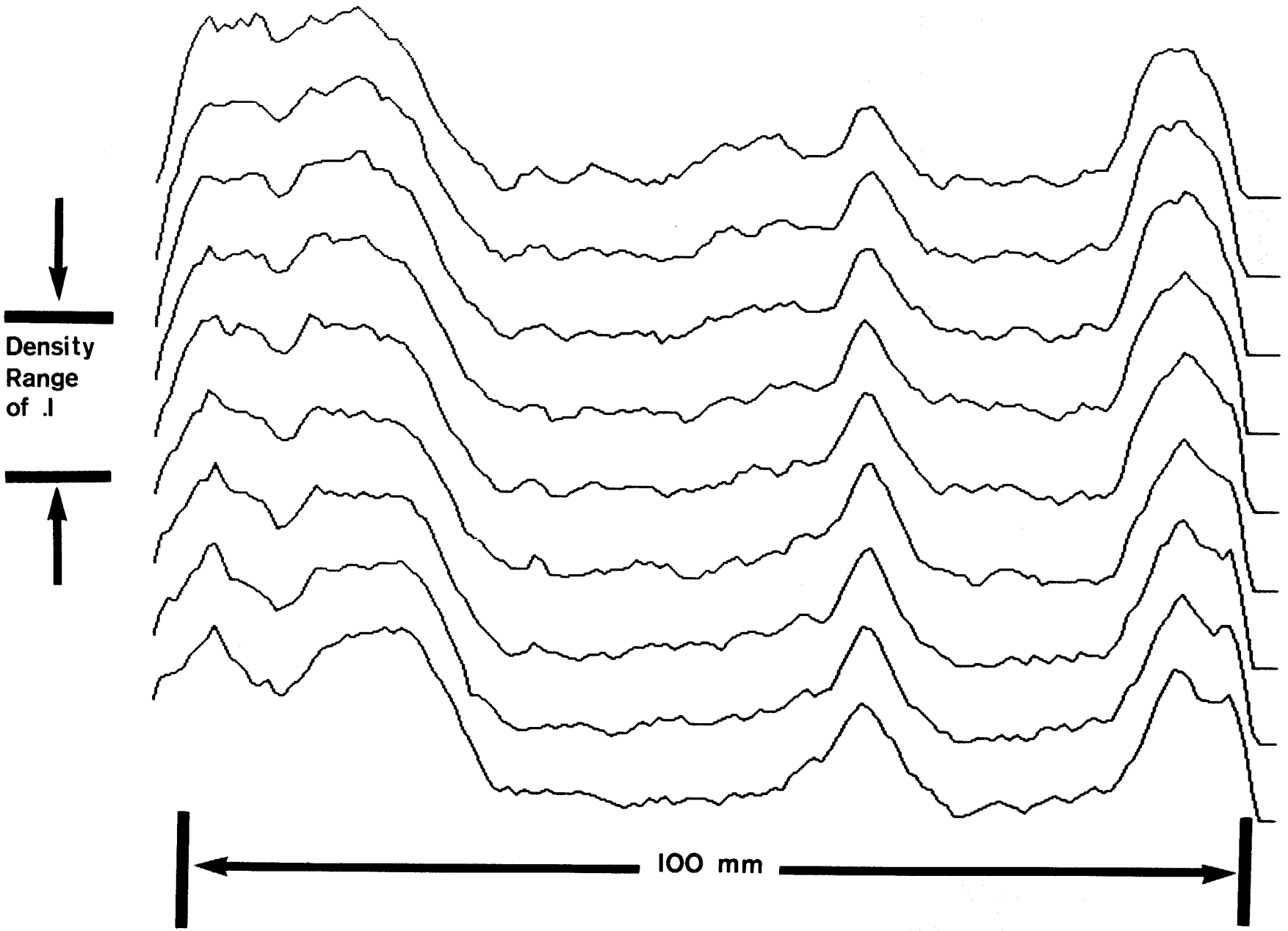
Density
Range
of .1
100 mm

TOP LEFT

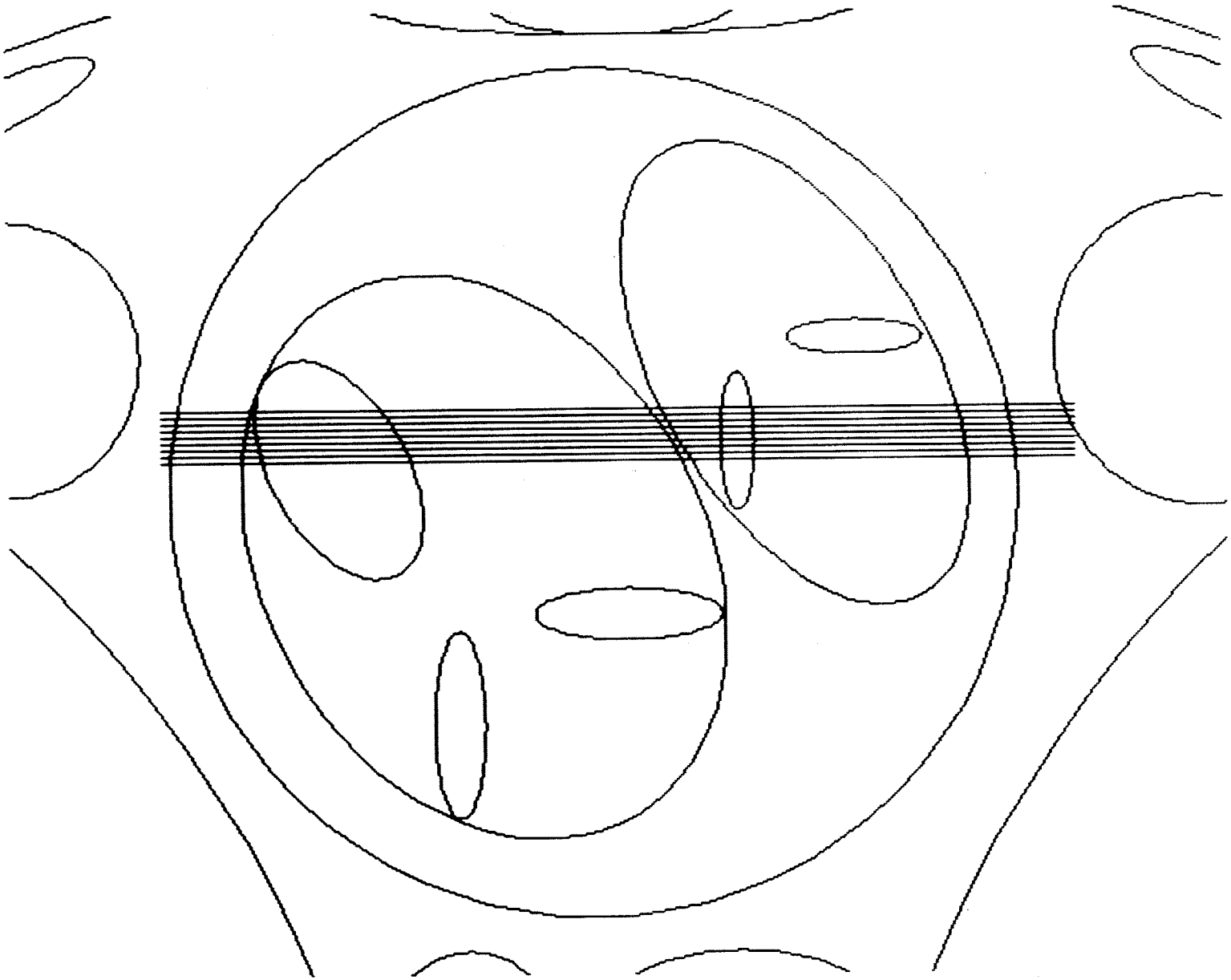

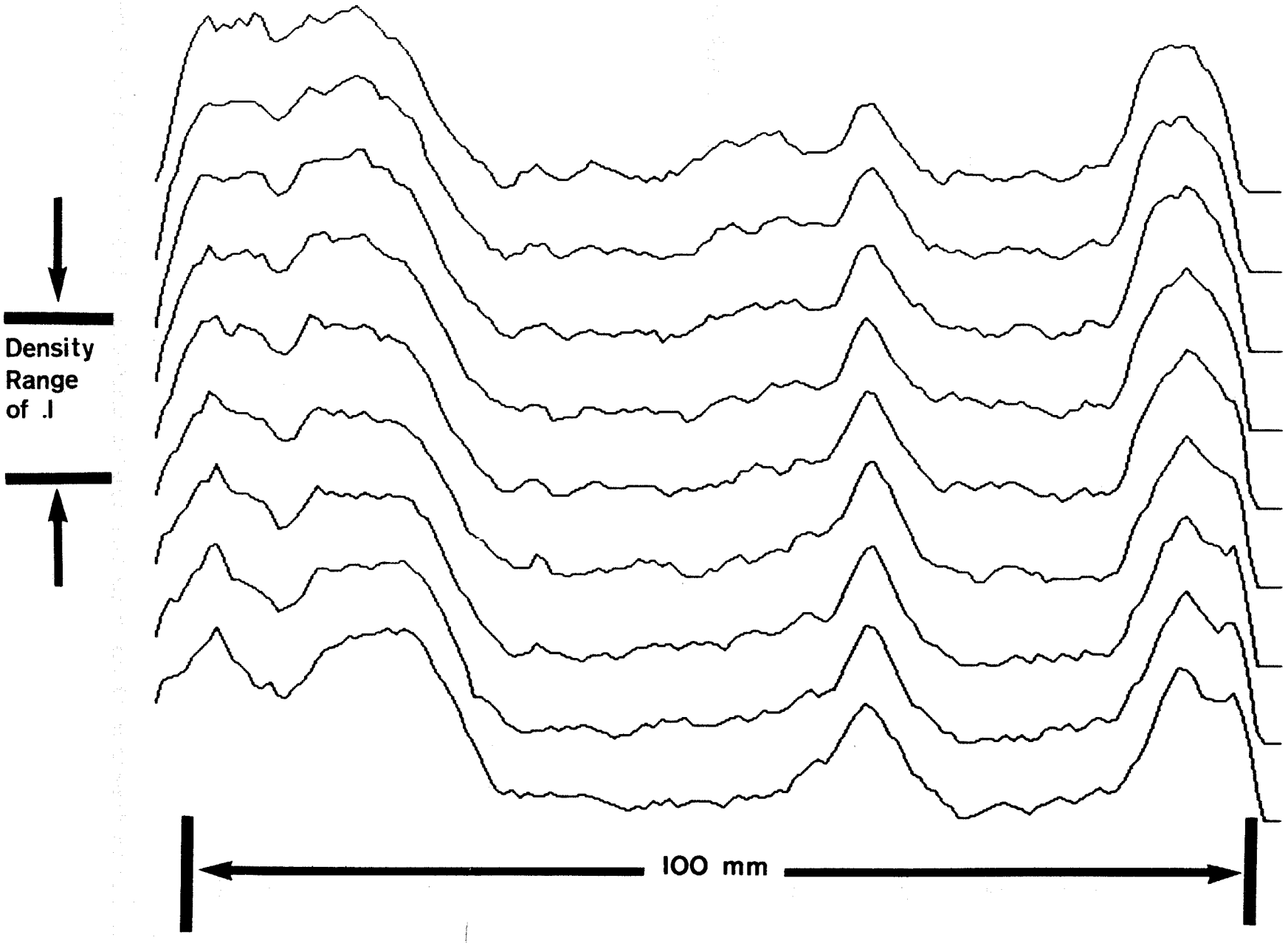
Density
Range
of .1
100 mm

TOP LEFT